sustainability

MDPI

Article

Field-Calibrated Sentinel-2 Assessment of Biomass and Carbon Storage in Mixed *Pinus halepensis–Cedrus atlantica* Stands Affected by Cedar Decline in Northeastern Algeria—A Sustainability Perspective

Oussama Meghithi [1,*], Toufik Aliat [1], Yassine Benabbes [1], Ahmed S. Abuzaid [2] and Mohamed S. Shokr [3,4,*]

[1] Higher National School of Forests, Khenchela 40000, Algeria; aliat.toufik@ensf.dz (T.A.); benabbes.yassine@ensf.dz (Y.B.)
[2] Soils and Water Department, Faculty of Agriculture, Benha University, Benha 13518, Egypt; ahmed.abuzaid@fagr.bu.edu.eg
[3] Soil and Water Department, Faculty of Agriculture, Tanta University, Tanta 31527, Egypt
[4] Institute of Environmental Engineering, RUDN University, Moscow 117198, Russia
* Correspondence: oussamameghi40@gmail.com (O.M.); mohamed_shokr@agr.tanta.edu.eg (M.S.S.)

Abstract

Reliable forest biomass and carbon-stock assessment is essential for climate-change mitigation and sustainable forest management, particularly in semi-arid Mediterranean mountain forests affected by drought, wildfire and tree decline. Here, we estimated above-ground biomass (AGB), total biomass, carbon stock and CO_2-equivalent storage in the Ouled Yagoub Forest, northeastern Algeria, by combining field inventory data, species-specific allometric equations, Sentinel-2 vegetation indices and elevation. We established 60 circular plots of 0.1 ha in April 2026 and retained 54 stocked plots for biomass modelling. The field inventory included 661 trees: 467 *Pinus halepensis* and 194 *Cedrus atlantica*, including 122 healthy and 72 declining cedar individuals. Field estimates indicated an AGB of 338.07 Mg, equivalent to 62.61 Mg ha^{-1} for stocked plots. Total biomass reached 436.11 Mg, while carbon stock and CO_2-equivalent storage reached 238.56 Mg C and 874.78 Mg CO_2eq, respectively. The NDVI-based model explained 78.3% of AGB variability, with Pearson's r = 0.885, RMSE = 48.77 Mg ha^{-1} and MAE = 39.14 Mg ha^{-1}. Cross-validation confirmed acceptable model stability, with LOOCV R^2 = 0.755 and RMSE = 51.86 Mg ha^{-1}, and 5-fold CV R^2 = 0.762 and RMSE = 51.07 Mg ha^{-1}. SAVI produced identical predictive performance because it was perfectly collinear with NDVI. Therefore, we selected the NDVI-only model as the most parsimonious model for spatial prediction. Declining *Cedrus atlantica* individuals showed lower estimated biomass and carbon storage than healthy cedar individuals, although this difference represents an observed pattern rather than a direct causal quantification of carbon loss due to dieback. The resulting maps provide field-calibrated exploratory spatial estimates rather than independently validated carbon maps. The research directly aligns with the principles of Sustainability, contributing to climate change mitigation and resilient forest management in semi-arid Mediterranean ecosystems. In addition, this work provides a stocked-plot carbon baseline and supports forest carbon monitoring, cedar conservation and restoration planning in the Aurès Mountains.

Keywords: forest biomass; carbon stock; Sentinel-2; NDVI; *Cedrus atlantica*; *Pinus halepensis*; cedar dieback; Ouled Yagoub Forest; semi-arid Mediterranean forest; Algeria

Check for updates

Academic Editor: Edgaras Linkevičius

Received: 10 June 2026
Revised: 9 July 2026
Accepted: 20 August 2026
Published: 26 August 2026

Copyright: © 2026 by the authors. Licensee MDPI, Basel, Switzerland. This article is an open access article distributed under the terms and conditions of the Creative Commons Attribution (CC BY) license.

1. Introduction

Forest biomass monitoring has become a key component of climate-change mitigation, greenhouse-gas reporting, and climate-smart forest management. Forest ecosystems store carbon in living above-ground biomass, below-ground biomass, litter, dead wood, and soils, thereby contributing directly to the regulation of atmospheric CO_2 concentrations [1,2]. Recent global carbon assessments emphasize that the land carbon sink remains a major component of the global carbon cycle, but its stability is increasingly affected by climate anomalies, droughts, fires, land-use change, and ecosystem degradation [3]. In addition, the interannual variability of terrestrial carbon exchange is strongly influenced by climatic fluctuations, particularly in semi-arid ecosystems, where small changes in water availability can produce large variations in carbon uptake and storage [4]. Therefore, accurate and spatially explicit estimation of forest above-ground biomass (AGB) and carbon stocks is essential for evaluating forest carbon-storage capacity and supporting national and regional carbon-accounting strategies [5].

Mediterranean mountain forests are particularly vulnerable to climate change because they are exposed to increasing aridity, recurrent droughts, wildfire disturbances, land degradation, and tree decline. Biomass and carbon storage in these ecosystems are highly heterogeneous due to variations in elevation, slope exposure, stand structure, species composition, soil conditions, and disturbance history [6]. In North Africa, *Cedrus atlantica* is one of the most ecologically and socio-economically important mountain conifers, but several studies have reported growth decline, dieback, and increased mortality associated with recurrent drought, aridification, anthropogenic pressure, and bark beetle outbreaks [7]. These disturbances may reduce forest productivity and carbon storage, making the quantification of biomass loss in declining cedar stands a relevant scientific and management priority [6].

Remote sensing provides a cost-effective and spatially continuous approach for estimating forest biomass, particularly when satellite observations are calibrated with field inventory data [8]. Sentinel-2 imagery is especially suitable for AGB estimation because it combines high spatial resolution, frequent revisit time, and multispectral information from visible, near-infrared, shortwave-infrared, and red-edge bands [9]. Vegetation indices derived from Sentinel-2 data can capture canopy greenness, vegetation vigour, chlorophyll content, water status, and soil-background effects. Recent studies have shown that the integration of Sentinel-2 spectral bands, vegetation indices, red-edge information, topographic variables, and machine-learning approaches can improve the accuracy of forest AGB estimation compared with models based only on simple vegetation indices [10].

However, the use of simple greenness indices alone may be insufficient in semi-arid Mediterranean forests. The Normalized Difference Vegetation Index (NDVI) is widely used to characterize canopy greenness and vegetation cover, but it may saturate in dense vegetation and can be affected by soil background in open or sparse stands [11]. The Soil Adjusted Vegetation Index (SAVI) was developed to reduce the influence of soil reflectance and is therefore useful in semi-arid forests where canopy cover is discontinuous [12]. Nevertheless, SAVI alone may still be unable to fully capture the complexity of forest biomass patterns because AGB is influenced not only by vegetation cover, but also by species composition, tree size distribution, canopy structure, topography, stand density, and disturbance history. In the present study, this issue was addressed by evaluating the performance of NDVI, SAVI, elevation, and their combined models [13].

In semi-arid Mediterranean mountain forests, biomass estimation cannot rely only on canopy greenness because forest structure is influenced by several interacting ecological, structural and environmental factors. (Ispikoudis et al. 2024) [14] showed that field measurements, allometric equations and geospatial techniques are useful for estimating

forest biomass and carbon storage in Mediterranean *Quercus ilex* ecosystems. Vegetation indices such as NDVI and SAVI provide useful information on canopy cover, vegetation vigour and soil-background effects, but biomass patterns are also affected by species composition, tree size distribution, stand density, topography, disturbance history and tree health status. (Song et al. 2024) [15] demonstrated that combining remote sensing data with environmental predictors such as topography, bioclimate and soil variables improves above-ground biomass estimation. Similarly, (Chen et al. 2025) [16] reported that Sentinel-2 spectral data alone may be limited in complex forest canopies, while integration with structural information improves the representation of spatial heterogeneity. Therefore, combining field inventory data with Sentinel-2 vegetation indices and elevation can provide a more ecologically meaningful framework for assessing forest biomass and carbon storage in heterogeneous mountain landscapes.

In Algeria, the Aurès Mountains constitute one of the main distribution areas of *Cedrus atlantica* and *Pinus halepensis*, two species of high ecological, socio-economic, and carbon-storage importance. The Ouled Yagoub Forest, located in Khenchela Province, represents a semi-arid Mediterranean montane ecosystem affected by drought, wildfire disturbance, canopy degradation, and Atlas cedar dieback. Despite its ecological importance, field-based and spatially explicit biomass and carbon-stock data remain limited for this forest, which restricts its integration into climate-smart forest management, restoration planning, and carbon-monitoring programmes. Moreover, few studies in the Aurès region have combined field inventory, species-specific allometric equations, Sentinel-2 vegetation indices, and cedar health status to quantify biomass and carbon-storage differences between healthy and declining trees. Species-specific carbon-stock parameters are particularly important for *Cedrus atlantica*, as El Mderssa et al. [17] reported a measured carbon fraction of 0.5643 tC tMS^{-1} for Atlas cedar, which is higher than the generic IPCC value of 0.51 tC tMS^{-1}.

Therefore, the objectives of this study were to: (i) estimate field-based AGB using species-specific allometric equations for *Pinus halepensis* and *Cedrus atlantica*; (ii) quantify total biomass, carbon stock and CO_2-equivalent storage from field inventory data; (iii) evaluate the relationship between field-estimated AGB and Sentinel-2-derived NDVI, SAVI and elevation; (iv) test model robustness using LOOCV and 5-fold cross-validation; (v) produce field-calibrated exploratory spatial estimates of AGB, carbon stock and CO_2-equivalent storage; and (vi) assess the observed difference in estimated biomass and carbon storage between healthy and declining *Cedrus atlantica* trees. The study provides a first field-based carbon-stock baseline for the Ouled Yagoub Forest, while the spatial maps are interpreted as exploratory outputs calibrated by field data rather than independently validated carbon maps.

2. Materials and Methods

The methodological workflow summarizes the main steps used to estimate and map AGB, carbon stock and CO_2-equivalent storage in the Ouled Yagoub Forest. We used a stratified field sampling design based on 60 circular plots of 0.1 ha to represent the main ecological and structural gradients of the forest, including species composition, elevation, canopy density, stand structure and cedar health condition. We retained 54 stocked plots for biomass modelling. In each plot, we recorded tree species, DBH, height and health status, then applied species-specific allometric equations to estimate plot-level AGB. In parallel, we processed Sentinel-2 Level-2A imagery to derive NDVI and SAVI, extracted elevation from a DEM, and harmonized all raster layers. We then extracted mean NDVI, SAVI and elevation values within each plot buffer and linked them to field-estimated AGB. Finally, we developed regression models, evaluated their performance using R^2, Pearson's correlation

coefficient, RMSE, MAE and SEE, and applied the most parsimonious NDVI-based model to produce exploratory maps of AGB, carbon stock and CO_2-equivalent storage (Figure 1).

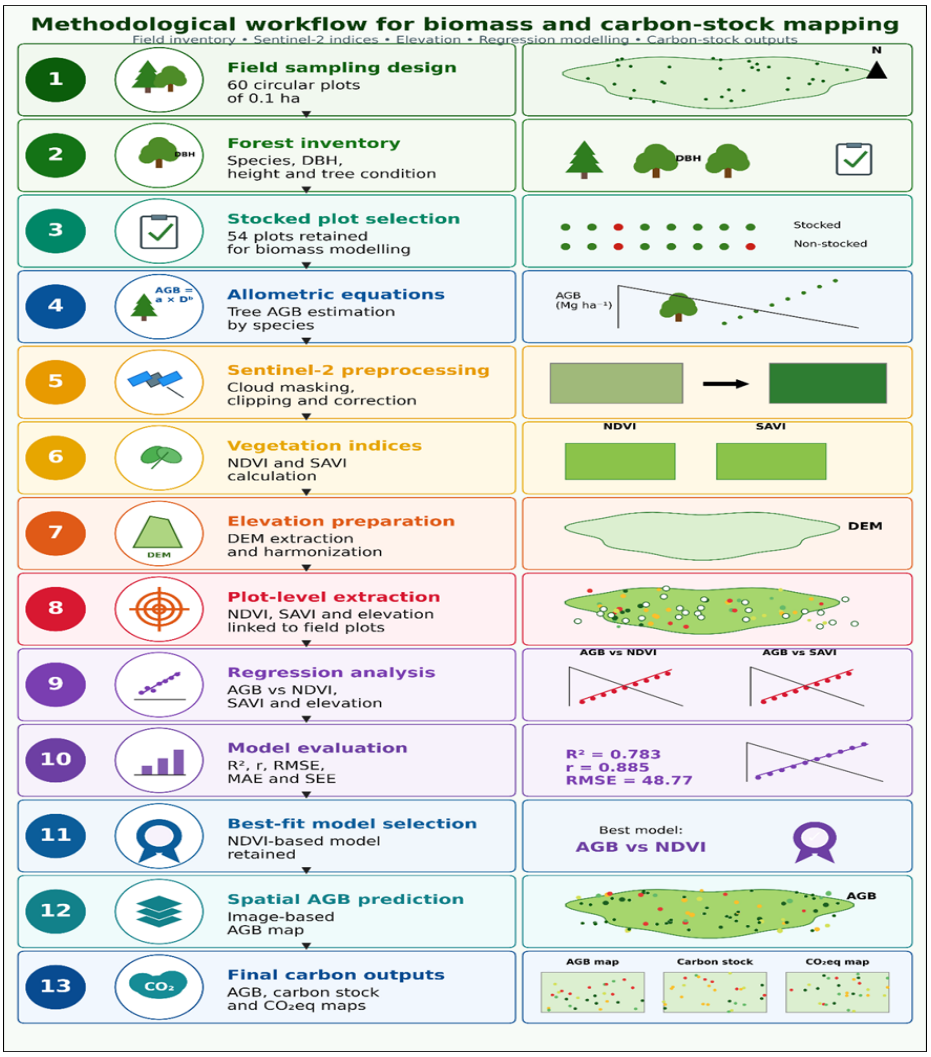


Figure 1. Methodological workflow for field-calibrated biomass and carbon-stock mapping in the Ouled Yagoub Forest. Arrows indicate the sequential workflow, while different colors distinguish the methodological steps.

The main abbreviations used in the manuscript are as follows: above-ground biomass (AGB); below-ground biomass (BGB); total biomass (TB); carbon dioxide equivalent (CO_2eq); Normalized Difference Vegetation Index (NDVI); Soil-Adjusted Vegetation Index (SAVI); root mean square error (RMSE); mean absolute error (MAE); standard error of estimate (SEE); leave-one-out cross-validation (LOOCV); and variance inflation factor (VIF).

2.1. Study Area

The study was conducted in the Ouled Yagoub Forest, located in the Aurès mountain massif, Wilaya of Khenchela, northeastern Algeria, between approximately 35°18′–35°27′ N and 006°37′–007°07′ E (Figure 2). The forest massif represents an important semi-arid Mediterranean montane ecosystem in northeastern Algeria and is characterized by a complex topography, heterogeneous forest formations, and strong altitudinal gradients [18,19]. Geospatial approaches including GIS-based land suitability analysis have been increasingly applied to assess forest site quality and biomass potential in semi-arid environments [20]. According to recent descriptions of the Ouled Yagoub State Forest, the broader forest massif

covers approximately 27,305 ha, with altitudes ranging from 869 m in the northern valley to more than 2170 m in the highest peaks [19]. To avoid confusion between the different surface values reported for the area, the value of approximately 27,305 ha refers to the broader Ouled Yagoub forest massif or administrative forest area, whereas the value of 18,671 ha corresponds to the mapped forest and shrubland formations reported in forest-formation datasets. Therefore, the first value describes the broader massif considered in this study, while the second value refers to the effective mapped vegetation formations within the forest landscape [19]. The climate is semi-arid Mediterranean, with cold wet winters, hot dry summers, and a marked seasonal drought. Mean annual precipitation is approximately 450.6 mm, while mean monthly temperatures range from about 1.9 °C in February to 35.7 °C in August. Based on the Emberger bioclimatic classification, the area belongs to the semi-arid bioclimatic stage with cool winters [19]. The soils are generally shallow and skeletal on steep slopes, while deeper soils occur in flatter areas. Lithosols and calcimorphic rendzina-type soils are common, particularly in limestone and marl-limestone formations [21].

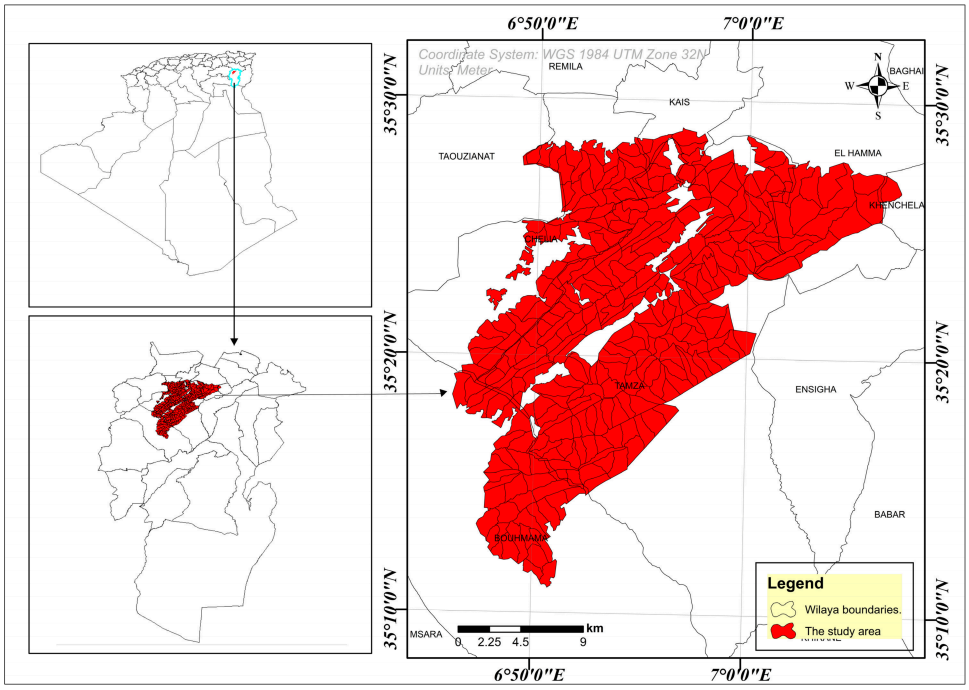


Figure 2. Geographical location of the Ouled Yagoub Forest in Khenchela Province, northeastern Algeria, adapted from Meghithi et al. [19]. The arrows indicate the successive localization of the study area from Algeria to Khenchela Province. The red polygon represents the Ouled Yagoub Forest study area, while the dashed lines indicate the geographic coordinate grid.

The vegetation is dominated by *Pinus halepensis* Mill. and *Cedrus atlantica Endl. Manetti*, associated with *Quercus ilex*, *Juniperus oxycedrus*, *Fraxinus* spp., shrublands, and wooded shrublands. *Pinus halepensis* mainly occupies lower and degraded slopes, generally between 1000 and 1400 m, whereas *Cedrus atlantica* occurs mostly in higher and relatively humid zones, from approximately 1400 to 2171 m [18]. The forest has also been affected by recurrent disturbances, including wildfire, grazing, soil erosion, and Atlas cedar dieback, which makes it a priority area for biomass and carbon stock assessment [7].

According to Chafai et al. [22], the Ouled Yagoub State Forest covers approximately 18,671 ha, of which 81% corresponds to forest formations and 19% to shrublands and wooded shrublands. Forest formations cover about 15,253 ha and are dominated by Atlas cedar (*Cedrus atlantica*), Aleppo pine (*Pinus halepensis*) and holm oak (*Quercus ilex*). Atlas

cedar represents one of the most emblematic vegetation types of the massif, with 3926 ha of mature cedar stands, including 3049 ha of dense formations. Mixed cedar–holm oak stands cover 1181 ha, while dense mature cedar stands associated with holm oak and *Fraxinus dimorpha* cover 638 ha. Holm oak formations include open coppice formations, mature open stands and dense coppice formations, with a total area of 1179 ha. Aleppo pine formations include 993 ha of managed open stands, 216 ha of young open stands, 610 ha of open pole-stage stands, 1314 ha of managed dense stands, 1328 ha of young dense stands, 1849 ha of dense pole-stage stands and 270 ha of mature dense stands [18].

Shrublands and wooded shrublands occupy approximately 3293 ha. They are mainly dominated by holm oak and prickly juniper (*Juniperus oxycedrus*), with 1141 ha of open shrublands and 1053 ha of dense shrublands. Dense shrublands composed of holm oak, prickly juniper and ash cover 123 ha, while wooded shrublands dominated by holm oak occupy 976 ha. Reforestation areas remain limited and cover only 125 ha, mostly corresponding to dense pole-stage plantations [22].

The forest-distribution map highlights the predominance of wooded formations within the Ouled Yagoub massif and confirms the marked spatial heterogeneity of vegetation cover [19]. Dense and relatively continuous stands occur mainly in mountainous sectors, whereas peripheral zones show more open and fragmented vegetation. This spatial pattern reflects the combined influence of elevation, topography and local ecological conditions on forest structure. Atlas cedar is largely restricted to higher and relatively humid areas, often in association with holm oak, while Aleppo pine occupies a broader ecological range across the massif. Figure 3 shows the spatial distribution of forest formations in Khenchela Province and the delimitation of the Ouled Yagoub State Forest study area.

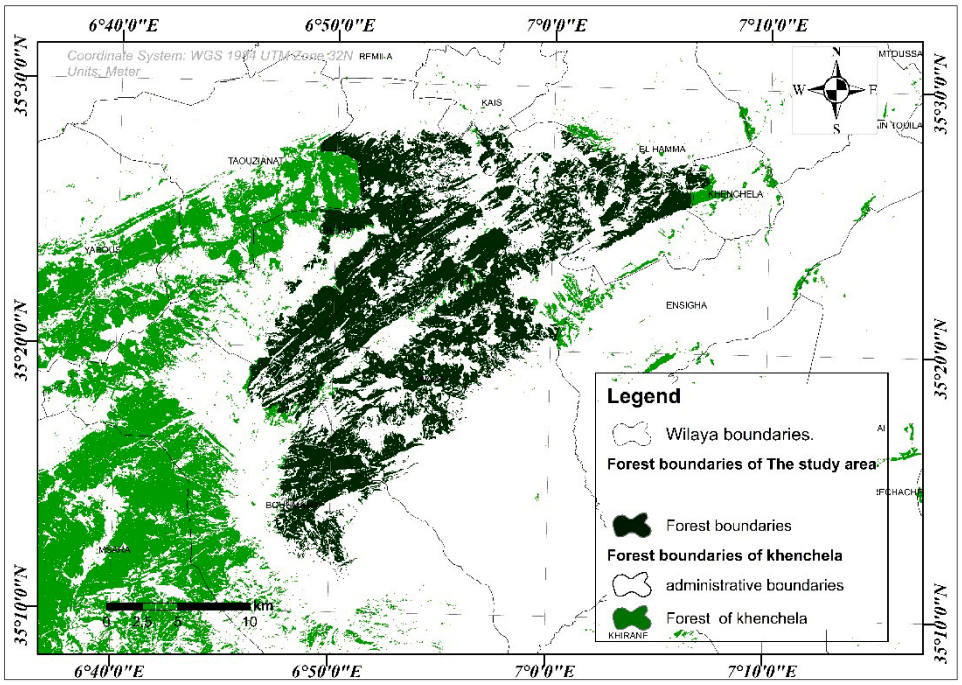


Figure 3. Spatial distribution of forest formations in Khenchela Province and delimitation of the Ouled Yagoub State Forest study area.

2.2. Relevance of the Ouled Yagoub Forest as a Natural Laboratory for Carbon-Stock Assessment

The Ouled Yagoub State Forest provides a suitable natural laboratory for forest carbon-stock assessment because it combines diverse forest formations, strong altitudinal gradients, variable stand densities and contrasting disturbance levels within a single mountainous landscape. Dense Atlas cedar stands, Aleppo pine forests, holm oak formations, shrublands,

burned areas and reforestation zones create contrasting conditions for biomass accumulation and carbon storage [22]. In addition, recurrent wildfire, drought stress and vegetation decline strongly affect forest productivity and carbon dynamics, making this massif an appropriate setting for analyzing AGB variability in semi-arid Mediterranean ecosystems [19]. These characteristics justify the integration of field inventory data, Sentinel-2 imagery and GIS-based carbon mapping in northeastern Algeria [18].

2.3. Field Data Acquisition

2.3.1. Sampling Design

We conducted the field campaign between 15 and 22 April 2026 in the Ouled Yagoub State Forest. We established 60 circular plots of 0.1 ha, corresponding to a radius of approximately 17.84 m. The stratified random sampling design captured the main ecological and structural gradients of the forest, including species composition, elevation, canopy density, stand structure and cedar health condition. We generated plot centres as random GPS coordinates within the forest boundary using ArcMap 10.8 (Esri, Redlands, CA, USA), while ensuring representation of the main forest formations and ecological conditions. Field teams navigated to each plot centre using handheld GPS receivers and recorded geographic coordinates after a stabilization period of approximately 3–5 min to minimize canopy-related positioning errors. We also recorded slope, aspect, dominant species, canopy conditions, and visible disturbance signs (Figure 4).

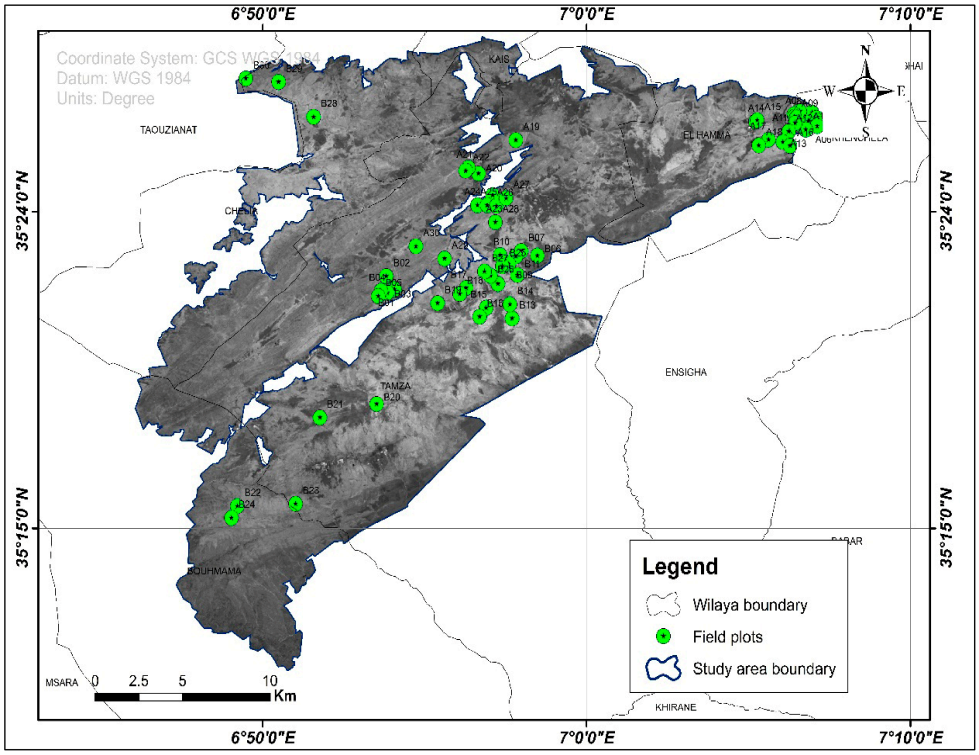


Figure 4. Spatial distribution of field inventory plots in the Ouled Yagoub Forest.

The distribution of field plots shows that the sampling design covered different sectors of the Ouled Yagoub Forest, including lower pine-dominated areas, central mixed forest formations, and higher cedar-dominated sectors. This spatial coverage was important for capturing the heterogeneity of forest structure, canopy condition, and biomass distribution. The plot network therefore provided a field basis for calibrating the relationship between Sentinel-2 vegetation indices and above-ground biomass.

The distribution of the 54 stocked plots retained for biomass modelling is summarized in Table 1. The plot network covered lower pine-dominated stands, intermediate mixed sectors and higher cedar-dominated sectors. Cedar health status was recorded at tree level rather than used as a plot-level stratification variable.

Table 1. Distribution of stocked plots according to dominant species group and elevation class.

Species Group	<1200 m	1200–1499 m	≥1500 m	Total Stocked Plots
Pinus halepensis	24	7	0	31
Cedrus atlantica	0	6	17	23
Total stocked plots	24	13	17	54

2.3.2. Tree Measurements and Atlas Cedar Health-Status Classification

Within each plot, all trees with a diameter at breast height (DBH) ≥ 7.5 cm were inventoried. Trees were included when more than 50% of their root collar was located inside the plot boundary, following an inclusive boundary rule. For each tree, species identity, DBH, total height, and health status were recorded. DBH was measured at 1.30 m above ground using a diameter tape, while total tree height was measured using a Blume-Leiss hypsometer (Figure 5).



Figure 5. Field measurement protocol—(**a**) DBH measurement with measuring tape at 1.30 m; (**b**) total height measurement with Blume-Leiss hypsometer; (**c**) identification of declining cedar (Ca.dep) by crown dieback and bark beetle galleries.

We coded tree species and health status as follows: Ph for *Pinus halepensis*, Ca for healthy *Cedrus atlantica* and Ca.dep for declining *Cedrus atlantica*. We assessed cedar health status visually in the field using crown condition and external decline symptoms. Healthy cedar trees showed dense green crowns, normal foliage density and no visible decline symptoms. Declining cedar trees showed crown dieback, partial defoliation, dead branches, reduced foliage density and, when present, bark beetle galleries or other signs of biotic damage. We treated cedar health status as a field-based categorical variable and applied the same diagnostic criteria consistently across all plots to reduce observer subjectivity. Because we did not measure detailed crown-dieback percentages, this visual classification represents a methodological limitation.

Among the 60 sampled plots, 54 contained trees above the minimum DBH threshold and entered the AGB estimation and regression analysis. The remaining six plots corresponded to treeless or severely degraded areas, mainly affected by recent wildfire, strong

vegetation degradation or very sparse tree cover. We excluded these plots from the primary regression calibration because the main model aimed to link Sentinel-2 vegetation indices to tree biomass in stocked forest plots. However, this exclusion may overestimate AGB in treeless, burned or highly degraded areas. Therefore, we interpret the spatial predictions as field-calibrated exploratory estimates rather than fully validated biomass maps. We also performed a sensitivity analysis by including these six plots as zero-AGB observations to evaluate their influence on model behaviour.

2.4. Field Above-Ground Biomass (AGB) Estimation Using Allometric Equations

We estimated field AGB using species-specific allometric equations applied to the dendrometric measurements collected in each plot. Allometric equations provide a non-destructive method for estimating tree biomass from measurable variables such as DBH and total tree height. We used species-specific equations because biomass allocation differs between Mediterranean conifers, particularly between *Pinus halepensis* and *Cedrus atlantica*. For *Pinus halepensis*, we applied the equation developed by Montero et al. [23], which was established for Mediterranean Aleppo pine stands. For *Cedrus atlantica*, we used the equation proposed by El Mderssa et al. [17], developed for Atlas cedar under North African forest conditions. We applied the same cedar equation to healthy and declining individuals because no specific allometric equation is currently available for declining *Cedrus atlantica*. This choice represents a major methodological limitation because crown dieback, partial mortality, branch loss and foliar reduction may alter biomass allocation, particularly in declining trees (Table 2).

Table 2. Allometric equations used for tree-level AGB estimation.

Species/Condition	Equations	Variables	Reference	*n*	R^2
Pinus halepensis	B (kg) = $\lambda \times \exp(-2.0939) \times DBH^{2.20988}$; $\lambda = \exp(0.1516^2/2) = 1.0115$	B = tree dry biomass; *DBH* = diameter at breast height, cm; λ = logarithmic bias-correction factor	[23]	55	0.982
Cedrus atlantica healthy	PST (kg) = $1.017 \times exp(4.5656) \times C^{2.1437} \times H^{0.4026}$; $C(m) = \pi \times DBH/100$	*PST* = tree dry biomass; *C* = circumference at breast height, *m*; *DBH* = *cm*; *H* = total height, *m*	[17]	60	0.981
Cedrus atlantica declining	Same equation as healthy *Cedrus atlantica*	*DBH*, *C*, *H* and health-status class	Adapted from [17]	—	—

Where B and PST represent individual tree dry biomass expressed in kg, DBH is the diameter at breast height measured at 1.30 m and expressed in cm, C is the circumference at breast height expressed in m, and H is total tree height expressed in m. For *Cedrus atlantica*, circumference was derived from DBH according to (Equation (1)):

$$C = \pi \times DBH / 100 \quad (1)$$

Tree-level *AGB* values were summed within each plot to obtain plot-level biomass. Since each circular plot covered 0.1 ha, plot biomass was converted to Mg ha^{-1} using (Equation (2)):

$$AGBplot = \frac{\Sigma AGBi}{(1000 \times 0.1)} \quad (2)$$

where AGBplot is the plot-level above-ground biomass expressed in Mg ha^{-1}, $\Sigma AGBi$ is the sum of individual tree biomass values expressed in kg, 1000 is the conversion factor from kg to Mg, and 0.1 corresponds to the plot area in hectares.

2.5. Carbon Stock and CO_2-Equivalent Calculation

Plot-level above-ground biomass was converted into below-ground biomass, total biomass, carbon stock, and CO_2-equivalent storage following the IPCC carbon-accounting framework and the species-specific parameters available for *Cedrus atlantica*. This conversion was applied first to field-estimated *AGB* values in order to quantify plot-level carbon storage. For spatial outputs, the same conversion procedure was applied to *AGB* values predicted by the selected *NDVI*-based model. Elevation was not used directly in the biomass-to-carbon conversion, but was retained as an ecological variable supporting the interpretation of biomass patterns along the altitudinal gradient.

Below-ground biomass was estimated using a root-to-shoot ratio of 0.29. Total biomass was calculated as the sum of above-ground and below-ground biomass.

We calculated the biomass-to-carbon conversion chain as follows (Equations (3)–(6)):

$$BGB = R \times AGB \; (R = 0.29) \tag{3}$$

$$TB = AGB + BGB \tag{4}$$

$$C = FC \times TB \; \left(FC_{pine} = 0.50;\; FC_{cedar} = 0.5643\right) \tag{5}$$

$$CO_2eq = C \times 3.667 \tag{6}$$

where *AGB* is above-ground biomass, *BGB* is below-ground biomass, TB is total biomass, C is carbon stock, FC is the biomass-to-carbon conversion factor, and CO_2eq is carbon dioxide-equivalent storage. The factor 3.667 corresponds to the molecular mass ratio of CO_2 to C, equal to 44/12.

Carbon stock was calculated separately for each species before being summed at plot level. This procedure avoided the use of a single generic carbon fraction for all trees and allowed the higher measured carbon fraction of *Cedrus atlantica* to be represented in the final carbon-stock estimates. For *Cedrus atlantica*, a species-specific carbon fraction of 0.5643 tC tDM^{-1} was used, whereas a carbon fraction of 0.50 was applied for *Pinus halepensis*. The resulting carbon-stock and CO_2-equivalent values should be interpreted as model-based estimates rather than direct measurements of carbon content, because root-to-shoot ratios and carbon fractions may vary according to species, tree age, site conditions and health status.

Elevation was not used in the biomass-to-carbon conversion itself. The carbon-stock and CO_2-equivalent maps were derived from the selected *NDVI*-based *AGB* model. Elevation was retained only as an ecological variable supporting the interpretation of biomass patterns along the altitudinal gradient.

We used Sentinel-2 MSI imagery to derive spectral predictors for AGB and carbon-stock modelling in the Ouled Yagoub State Forest. We selected Sentinel-2 data because they provide high spatial resolution, frequent revisit time and spectral sensitivity to canopy greenness, vegetation structure and biomass-related variability. We selected the satellite image as close as possible to the field campaign conducted between 15 and 22 April 2026 to ensure temporal consistency between dendrometric measurements and satellite-derived spectral information. We retained a Sentinel-2 Level-2A surface reflectance image acquired on 16 April 2026 and considered only images with cloud cover lower than 10%. We processed the image in Google Earth Engine using the COPERNICUS/S2_SR_HARMONIZED collection. We applied cloud and cloud-shadow masking using the Scene Classification Layer (SCL). We used the red band (B4) and near-infrared band (B8), both at 10 m spatial resolution, to calculate *NDVI* and *SAVI*. We extracted elevation from a digital elevation model and harmonized it with the Sentinel-2-derived raster layers before plot-level ex-

traction. We extracted mean *NDVI*, *SAVI* and elevation values within circular plot buffers corresponding to the field-plot radius of 17.84 m.

The main characteristics of the Sentinel-2 image used in this study are summarized in Table 3.

Table 3. Sentinel-2 image used for biomass and carbon-stock modelling.

Parameter	Description
Satellite sensor	Sentinel-2 MSI
GEE collection	COPERNICUS/S2_SR_HARMONIZED
Product level	Level-2A surface reflectance
Acquisition date	16 April 2026
Field campaign period	15–22 April 2026
Spatial resolution	10–20 m
Cloud cover threshold	<10%
Cloud and shadow masking	Scene Classification Layer (SCL)
Spectral bands used	Red band B4 and near-infrared band B8
Derived indices	NDVI and SAVI
DEM source	SRTM 30 m DEM
Plot extraction method	Mean raster values extracted within 17.84 m circular plot buffers
Processing platform	Google Earth Engine
GIS software	ArcMap 10.8
Purpose	Extraction of spectral and topographic predictors for AGB modelling

We performed image preprocessing in Google Earth Engine (GEE). The workflow included cloud and cloud-shadow masking, selection of the relevant spectral bands, and clipping of the image to the Ouled Yagoub Forest boundary. The Level-2A product corresponds to atmospherically corrected bottom-of-atmosphere surface reflectance; therefore, no additional atmospheric correction was required.

We calculated *NDVI* using the red and near-infrared bands, while *SAVI* was derived to reduce the influence of exposed soil and soil-background reflectance in open-canopy semi-arid forest conditions. We exported the resulting *NDVI* and *SAVI* raster layers to ArcMap for plot-level extraction, spatial analysis and cartographic production [24].

The processed Sentinel-2 dataset provided consistent spectral predictors for subsequent regression modelling. We evaluated *NDVI* and SAVI as predictors of *AGB*. Because both indices showed identical predictive performance and strong collinearity, we used the most parsimonious *NDVI*-based model for final spatial prediction, while retaining elevation as an ecological variable to support the interpretation of biomass distribution.

2.6. Vegetation Indices

2.6.1. Normalized Difference Vegetation Index (*NDVI*)

NDVI is one of the most widely used spectral indices for characterizing canopy greenness, vegetation density, and photosynthetic activity. It exploits the contrast between red reflectance, which decreases with chlorophyll absorption, and near-infrared reflectance, which increases with healthy leaf structure. In forest environments, *NDVI* provides a useful proxy for canopy condition and biomass-related spatial variability, although its

performance may be affected by saturation in dense canopies and by soil background in sparse or open stands [19].

We calculated *NDVI* as follows (Equation (7)):

$$NDVI = \frac{NIR - Red}{NIR + Red} \quad (7)$$

In this equation, *NIR* is near-infrared reflectance, and Red is red reflectance. The *NDVI* values theoretically vary from −1 to +1, where higher values correspond to denser and more vigorous vegetation cover and lower values correspond to sparse vegetation, degraded forest cover, bare soil, or non-vegetated surfaces.

2.6.2. Soil-Adjusted Vegetation Index (*SAVI*)

SAVI reduces the influence of soil background on vegetation reflectance and is particularly relevant in semi-arid Mediterranean forests, where open canopies, sparse vegetation and exposed soil can affect spectral response. The index incorporates a soil-adjustment factor that improves vegetation-cover detection under low to moderate canopy-density conditions compared with *NDVI* [12]. Soil-adjusted indices such as *SAVI*, *MSAVI* and *OSAVI* are useful for assessing vegetation structure and exposed-soil surfaces in semi-arid forest environments [19].

We calculated *SAVI* as follows (Equation (8)):

$$SAVI = \left[\frac{(NIR - Red)}{(NIR + Red + L)}\right] \times (1 + L) \quad (8)$$

where *NIR* represents the near-infrared reflectance, Red represents the red reflectance, and L is the soil-adjustment factor. In this study, L = 0.5 was used, as it is commonly recommended for intermediate vegetation-cover conditions.

Higher *SAVI* values generally indicate denser and healthier vegetation cover, whereas lower values correspond to sparse vegetation, degraded forest stands, exposed soil, or non-vegetated surfaces.

2.6.3. Extraction of Plot-Level Spectral Values

We used the *NDVI* and *SAVI* raster layers as explanatory variables for *AGB* and carbon-stock modelling. For each field plot, we extracted vegetation-index values from Sentinel-2 raster layers and linked them to plot-level *AGB* values derived from species-specific allometric equations. Because each plot covered 0.1 ha, corresponding to a radius of 17.84 m, we extracted spectral information using a circular plot buffer rather than a single central pixel [13]. This approach improved spatial correspondence between field measurements and satellite observations, reduced the influence of GPS positional error, and limited mixed-pixel effects in heterogeneous forest stands [9].

In semi-arid Mediterranean forests, discontinuous canopy cover and exposed soil can influence the spectral signal. Therefore, extracting mean spectral values within the plot area provides more representative vegetation-index values than relying on single-pixel extraction [11]. For each stocked plot, we calculated mean *NDVI* and *SAVI* values within the corresponding 0.1 ha buffer and assigned them to the plot-level biomass database.

We then compared the extracted *NDVI* and *SAVI* values with field-estimated *AGB* expressed in Mg ha^{-1}. Regression analysis evaluated the relationship between satellite-derived vegetation indices, elevation and field-based biomass estimates. Because *NDVI* and *SAVI* showed identical predictive performance and strong collinearity, we used the most parsimonious *NDVI* model for spatial prediction and retained elevation mainly as an ecological variable supporting the interpretation of biomass distribution.

2.6.4. Software and Spatial Analysis

All remote-sensing preprocessing steps were carried out in Google Earth Engine, a cloud-based geospatial platform that enables efficient processing of large satellite datasets and reproducible vegetation-index computation [24]. Sentinel-2 Level-2A surface reflectance imagery was clipped to the Ouled Yagoub Forest boundary, and *NDVI* and *SAVI* were computed pixel by pixel using the red and near-infrared bands. The use of atmospherically corrected Sentinel-2 Level-2A data ensured that vegetation indices were derived from bottom-of-atmosphere surface reflectance, improving the consistency of spectral values used for biomass modelling.

The resulting vegetation-index rasters were exported from Google Earth Engine and integrated into a GIS environment for spatial analysis. ArcMap was used for plot-buffer creation, raster value extraction, linkage between field and satellite datasets, regression output management, and final map production. GIS-based extraction allowed each field plot to be associated with its corresponding mean *NDVI* and *SAVI* values, thereby creating a unified plot-level database combining field inventory measurements, allometric biomass estimates, and satellite-derived predictors.

Final spatial outputs included maps of *NDVI*, *SAVI*, predicted above-ground biomass, carbon stock, and CO_2-equivalent storage. These maps were produced at the study-area scale to support the interpretation of spatial patterns in forest biomass and carbon storage. The integration of field inventory data, species-specific allometric equations, Sentinel-2 vegetation indices, and GIS-based spatial analysis provided a consistent methodological framework for mapping forest biomass and carbon stocks in the semi-arid Mediterranean conditions of the Ouled Yagoub Forest. Similar cloud-based and GIS-integrated workflows have been used in recent forest-monitoring studies to process multispectral satellite imagery, derive vegetation indices, and support spatial interpretation of forest disturbance, vegetation condition, and biomass-related variables.

2.7. Elevation Extraction and Topographic Predictor Preparation

We integrated elevation as a topographic variable to support the ecological interpretation of *AGB* distribution. In mountainous semi-arid Mediterranean forests, elevation influences temperature regime, moisture availability, soil depth, species distribution, stand structure and disturbance intensity. Therefore, we considered elevation an ecologically relevant variable for explaining *AGB* variability in the Ouled Yagoub Forest. We assigned plot-level elevation values to each field plot and combined them with Sentinel-2-derived *NDVI* and *SAVI* values. For spatial modelling, we derived the elevation layer from a digital elevation model and harmonized it with the Sentinel-2 raster layers using the same projection, spatial extent, spatial resolution and pixel alignment. The final predictor set included *NDVI*, *SAVI* and elevation.

2.8. Statistical Analysis and Model Evaluation

We used correlation and regression analyses to evaluate the relationship between field-estimated *AGB* and spectral and topographic predictors. Plot-level *AGB*, expressed in Mg ha^{-1}, served as the dependent variable, while *NDVI*, *SAVI* and elevation served as explanatory variables. We conducted the analysis using the 54 stocked plots retained for biomass estimation.

First, we fitted simple linear regression models separately for *NDVI*, *SAVI* and elevation. Second, we tested multiple linear regression models using different predictor combinations: *NDVI* + *SAVI*, *NDVI* + *elevation*, *SAVI* + elevation and *NDVI* + *SAVI* + elevation. This modelling strategy evaluated whether elevation added predictive value compared with vegetation-index-only models.

Because *NDVI* and *SAVI* showed identical predictive performance and strong collinearity, we selected the final model using a parsimonious approach. We retained the *NDVI*-based model for spatial *AGB* estimation because it provided strong predictive performance while avoiding redundant predictors. We retained elevation for ecological interpretation rather than as a dominant predictive variable. The general form of the simple regression model was expressed as follows (Equation (9)):

$$AGB = \beta^0 + \beta^1 X + \varepsilon \quad (9)$$

where *AGB* is above-ground biomass expressed in Mg ha^{-1}, X represents one explanatory variable, either *NDVI*, *SAVI*, or elevation, β_0 is the intercept, β_1 is the regression coefficient, and ε is the residual error.

The general form of the multiple regression model was expressed as follows (Equation (10)):

$$AGB = \beta^0 + \beta^1 NDVI + \beta^2 SAVI + \beta^3 Elevation + \varepsilon \quad (10)$$

where NDVI and SAVI represent Sentinel-2 vegetation indices, and Elevation represents the plot-level altitude expressed in metres.

Model performance was evaluated using the coefficient of determination (R^2), adjusted R^2, root mean square error (*RMSE*), standard error of the estimate (*SEE*), and Pearson correlation coefficient for simple models or multiple correlation coefficient for multiple models. R^2 and adjusted R^2 were used to assess the proportion of *AGB* variability explained by each model, while RMSE and *SEE* were used to quantify prediction error [25]. Similar performance metrics are commonly used in field-calibrated biomass and carbon-stock modelling studies based on remote sensing and inventory data [9].

RMSE was calculated as follows (Equation (11)):

$$RMSE = \sqrt{\left[\frac{\left(\Sigma(yi - \hat{y}i)^2\right)}{n}\right]} \quad (11)$$

And *SEE* was calculated as follows (Equation (12)):

$$SEE = \sqrt{\left[\frac{\left(\Sigma(yi - \hat{y}i)^2\right)}{(n - p - 1)}\right]} \quad (12)$$

where yi represents observed field-estimated *AGB*, ŷi represents model-predicted *AGB*, n is the number of plots, and p is the number of explanatory variables included in the model.

Because *NDVI* and *SAVI* showed identical performance and strong collinearity, the final model was selected using a parsimonious approach. The *NDVI*-based model was retained for spatial *AGB* estimation because it provided strong predictive performance while avoiding redundant predictors. Elevation was retained for ecological interpretation rather than as a dominant predictive variable. This cautious interpretation is important because biomass estimation based on field inventory, allometric equations, vegetation indices, and environmental predictors remains model-dependent and should be validated with independent field data. The use of species-specific biomass and carbon parameters is also important, particularly for *Cedrus atlantica*, for which El Mderssa et al. reported a measured carbon fraction of 0.5643 tC tMS^{-1}, higher than the generic IPCC value of 0.51 tC tMS^{-1} (Table 4).

Table 4. Regression models tested for AGB prediction.

Model Type	Predictors	Purpose
Simple regression	*NDVI*	Test the relationship between canopy greenness and AGB
Simple regression	*SAVI*	Test the influence of soil-adjusted vegetation cover on AGB
Simple regression	Elevation	Test the topographic control on AGB
Multiple regression	*NDVI* + *SAVI*	Evaluate vegetation-index-only performance
Multiple regression	*NDVI* + elevation	Test whether elevation improves the NDVI model
Multiple regression	*SAVI* + elevation	Test whether elevation improves the SAVI model
Multiple regression	*NDVI* + *SAVI* + elevation	Identify the best spectral-topographic exploratory model

2.9. Model Validation and Collinearity Diagnostics

To strengthen model validation, the regression models were evaluated using both calibration statistics and cross-validation. Cross-validation is widely used to assess predictive ability and reduce the risk of overfitting, particularly when models are developed from limited datasets (Stone, 1974; Arlot and Celisse, 2010) [26,27]. Model calibration was assessed using Pearson's correlation coefficient, R^2, *RMSE*, MAE and SEE. These accuracy metrics are commonly used to evaluate agreement between observed and predicted forest above-ground biomass estimates derived from remote-sensing models (Valbuena et al., 2017) [28]. In addition, two cross-validation procedures were applied: leave-one-out cross-validation (LOOCV) and 5-fold cross-validation. LOOCV was used because it allows each observation to be used once as a validation case, while 5-fold cross-validation provided an additional estimate of prediction stability (Stone, 1974; Arlot and Celisse, 2010) [26,27]. Cross-validated R^2 was calculated from observed and predicted AGB values as *RMSE*, *MAE* and bias were also calculated from the cross-validated predictions.

To address multicollinearity between predictors, a Pearson correlation matrix and variance inflation factors (VIF) were calculated for *NDVI*, *SAVI* and elevation. VIF is commonly used to diagnose multicollinearity in regression models, but its interpretation should consider sample size, model structure and the analytical context (O'Brien, 2007; Thompson et al., 2017) [29,30]. Because *NDVI* and *SAVI* were perfectly collinear in the plot dataset, they were not retained together in the same final regression model.

3. Results and Discussion

3.1. Dendrometric Structure and Field-Derived Above-Ground Biomass

The field inventory included 661 trees distributed among three species/health-status groups: 467 individuals of *Pinus halepensis*, 122 healthy individuals of *Cedrus atlantica*, and 72 declining individuals of *Cedrus atlantica*. The dendrometric characteristics of the sampled trees are summarized in Table 5.

Table 5. Dendrometric characteristics and mean above-ground biomass of the sampled trees in the Ouled Yagoub Forest, April 2026.

Species	*n*	DBH Mean (cm)	DBH Min (cm)	DBH Max (cm)	DBH SD (cm)	H Mean (m)	H Max (m)	Mean AGB/Tree (kg)
Pinus halepensis	467	25.48	13.0	64.0	10.24	11.34	24.14	194.7
Cedrus atlantica healthy	122	59.96	12.0	130.5	31.47	14.99	28.00	1572.4
Cedrus atlantica declining	72	40.25	11.0	121.0	25.56	15.60	23.17	768.3

The results show clear structural differences among species and health-status classes. Healthy *Cedrus atlantica* trees exhibited the highest mean DBH and the highest mean above-ground biomass per tree, whereas declining cedar individuals showed lower DBH and lower biomass values. *Pinus halepensis* represented the largest number of measured trees but had lower mean DBH, height, and individual biomass compared with cedar trees [6] (Figure 6).

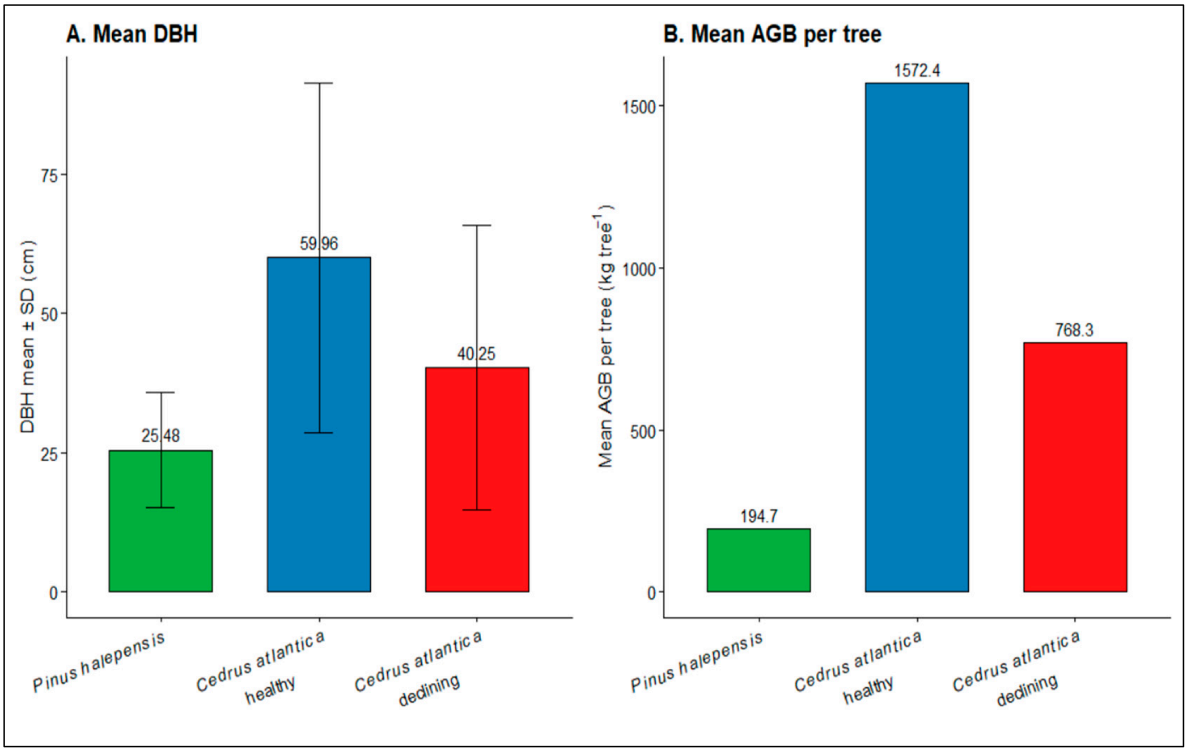


Figure 6. Species-level variation in mean diameter at breast height and above-ground biomass per tree in the Ouled Yagoub Forest. (**A**) Mean diameter at breast height (DBH ± SD) and (**B**) mean above-ground biomass (AGB) per tree for *Pinus halepensis*, healthy *Cedrus atlantica*, and declining *Cedrus atlantica*.

The comparison of dendrometric characteristics and individual above-ground biomass revealed that healthy *Cedrus atlantica* trees stored the highest mean AGB per tree, reaching 1572.4 kg tree^{-1}. Declining *Cedrus atlantica* individuals stored 768.3 kg tree^{-1}, indicating a reduction of approximately 51% compared with healthy cedar trees. In contrast, *Pinus halepensis* showed the lowest mean AGB per tree, with 194.7 kg tree^{-1}, despite being the most abundant species in the inventory [23].

These results indicate that healthy Atlas cedar trees contribute disproportionately to above-ground biomass storage because of their larger stem diameter and higher individual biomass [5]. The lower biomass observed in declining cedar trees suggests that health status may influence biomass accumulation and carbon storage, which is consistent with previous studies reporting growth decline, dieback, and productivity reduction in drought-stressed Atlas cedar forests [7]. This structural contrast also supports the use of species-specific allometric equations for estimating forest biomass and carbon stocks, because biomass allocation varies among species, tree size classes, and ecological conditions [17].

3.2. Field-Derived Above-Ground Biomass by Species and Plot

Species-specific allometric equations applied to the 54 stocked plots yielded a total AGB of 338.07 Mg over the sampled area. *Pinus halepensis* contributed 90.93 Mg, represent-

ing 26.9% of total AGB, whereas *Cedrus atlantica* contributed 247.14 Mg, corresponding to 73.1% of total AGB. Although cedar trees were less abundant than pine trees, they stored the dominant biomass share because they had larger stem diameters and higher individual biomass. Healthy *Cedrus atlantica* showed the highest mean AGB per tree (1572.4 kg tree^{-1}), followed by declining *Cedrus atlantica* (768.3 kg tree^{-1}) and *Pinus halepensis* (194.7 kg tree^{-1}). Declining cedar individuals therefore showed approximately 51% lower mean biomass than healthy cedar trees. This difference should be interpreted cautiously because tree size, age, site conditions and the use of the same allometric equation for healthy and declining cedar may influence the comparison.

At plot level, AGB showed strong spatial variability, ranging from low values in sparse or degraded plots to high values in cedar-dominated stands with large-diameter trees. The mean field-derived AGB was 62.61 Mg ha^{-1}, reflecting the heterogeneous structure of the Ouled Yagoub Forest, where young pine stands, open formations, declining cedar patches, and mature cedar stands coexist within the same massif (Table 6).

Table 6. Field-derived above-ground biomass by species in the Ouled Yagoub Forest, April 2026.

Species	N Trees	Total AGB (Mg)	AGB (Mg ha^{-1})	Mean AGB/Tree (kg)
Pinus halepensis	467	90.93	16.84	194.7
Cedrus atlantica healthy	122	191.83	—	1572.4
Cedrus atlantica declining	72	55.32	—	768.3
Cedrus atlantica total	194	247.14	45.77	1273.9
All species	661	338.07	62.61	511.5

The per-hectare field values reported in this section were calculated only for the 54 stocked plots retained for biomass modelling. Therefore, they represent a stocked-plot carbon baseline rather than a mean carbon stock for the entire forest area. Treeless and severely degraded plots were not included in the primary per-hectare field estimate, and this limitation should be considered when interpreting the spatial carbon baseline. The DBH class distribution showed a clear dominance of small to medium diameter classes, indicating an uneven-aged and structurally heterogeneous forest stand. *Pinus halepensis* was mainly concentrated in the 10–50 cm DBH classes, with the highest number of individuals recorded between 10 and 30 cm. In contrast, *Cedrus atlantica* displayed a wider DBH distribution, extending from small diameter classes to larger classes above 100 cm. This pattern reflects differences in stand structure, growth stage, and ecological status between the two species (Figure 5).

The dominance of smaller DBH classes, particularly for *Pinus halepensis*, suggests active regeneration or a relatively young stand structure. In contrast, the broader DBH distribution of *Cedrus atlantica*, including large-diameter individuals, indicates the presence of older trees and highlights the structural importance of cedar stands in the Ouled Yagoub Forest. This interpretation is consistent with the field inventory, where *P. halepensis* was numerically dominant but showed lower mean DBH and lower mean AGB per tree, whereas healthy *C. atlantica* showed the highest mean DBH and individual biomass (Figure 7).

This diameter structure is particularly important for biomass and carbon-stock estimation because larger trees contribute disproportionately to above-ground biomass. In the present study, healthy *C. atlantica* trees had a mean DBH of 59.96 cm and a mean AGB of 1572.4 kg tree^{-1}, whereas *P. halepensis* had a mean DBH of 25.48 cm and a mean AGB of only 194.7 kg tree^{-1}. This confirms that cedar trees, especially large healthy individuals, play a key role in forest biomass storage despite being less abundant than Aleppo pine.

The strong relationship between tree diameter and biomass is also supported by allometric biomass studies. Montero et al., [23] developed biomass and CO_2-fixation models using destructive sampling and dry-matter determination, showing that allometric models linking tree diameter to dry biomass are essential for forest carbon assessment. Similarly, ref. [17] emphasized the importance of species-specific biomass and carbon parameters for *Cedrus atlantica*, confirming that cedar biomass and carbon-stock estimation should rely on adapted dendrometric relationships rather than generic assumptions.

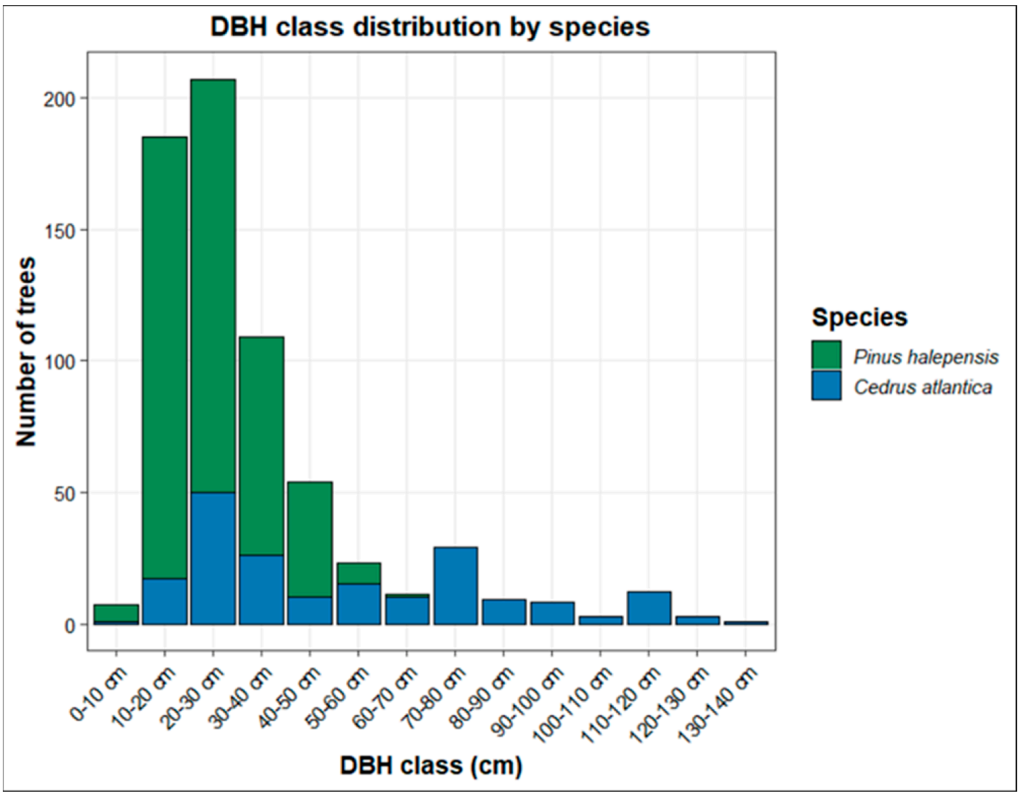


Figure 7. DBH class distribution of measured trees by species in the Ouled Yagoub Forest. Diameter classes were grouped into 10 cm intervals. The stacked bar chart shows the dominance of small to medium DBH classes for *Pinus halepensis* and a wider DBH range for *Cedrus atlantica*, reflecting differences in stand structure and development stages between the two species.

3.3. AGB Modelling with NDVI, SAVI and Elevation

Regression analysis showed a strong relationship between field-estimated aboveground biomass and Sentinel-2 vegetation indices. The NDVI-based model explained 78.3% of AGB variability, with Pearson's r = 0.885, RMSE = 48.77 Mg ha^{-1}, MAE = 39.14 Mg ha^{-1}, and SEE = 49.70 Mg ha^{-1}. The SAVI-based model produced exactly the same statistical performance, indicating that SAVI did not provide additional independent information compared with NDVI in the present dataset. Calibration and cross-validation performances of the tested models are summarized in Table 7.

Cross-validation confirmed the stability of the NDVI-based AGB model. The calibration performance was high, with R^2 = 0.783, RMSE = 48.77 Mg ha^{-1}, MAE = 39.14 Mg ha^{-1} and Pearson's r = 0.885. The LOOCV results remained close to the calibration statistics, with R^2 = 0.755 and RMSE = 51.86 Mg ha^{-1}, while 5-fold cross-validation produced R^2 = 0.762 and RMSE = 51.07 Mg ha^{-1}. The SAVI-based model produced identical results to the NDVI-based model, confirming redundancy between the two vegetation indices. The NDVI + Elevation model showed only a marginal improvement during calibration

but did not improve cross-validated performance. Therefore, the NDVI-only model was retained as the most parsimonious model for spatial AGB prediction.

The NDVI–SAVI correlation was 1.000, confirming perfect collinearity in the plot dataset. This occurred because NDVI and SAVI provided identical information across the 54 stocked plots. Therefore, SAVI did not provide additional independent information compared with NDVI in this dataset.

Table 7. Calibration and cross-validation performance of the tested AGB prediction models.

Model	Equation	n	Statistic	Calibration	LOOCV	5-Fold CV
NDVI-based AGB model	AGB = 607.21 × NDVI − 124.78	54	R^2	0.783	0.755	0.762
			RMSE	48.77	51.86	51.07
			MAE	39.14	41.14	40.68
			SEE	49.70	—	—
			r	0.885	—	—
			Bias	—	−0.99	−0.29
SAVI-based AGB model	AGB = 607.21 × SAVI − 100.49	54	R^2	0.783	0.755	0.762
			RMSE	48.77	51.86	51.07
			MAE	39.14	41.14	40.68
			SEE	49.70	—	—
			r	0.885	—	—
			Bias	—	−0.99	−0.29
Elevation-only model	AGB = 0.1361 × Elevation − 113.64	54	R^2	0.176	0.104	0.114
			RMSE	95.04	99.13	98.53
			MAE	58.14	60.66	61.23
			SEE	96.85	—	—
			r	0.420	—	—
			Bias	—	0.17	0.30
NDVI + Elevation model	AGB = 620.40 × NDVI − 0.0123 × Elevation − 111.87	54	R^2	0.784	0.747	0.757
			RMSE	48.65	52.64	51.66
			MAE	39.18	42.00	41.11
			SEE	50.06	—	—
			r	0.886	—	—
			Bias	—	−0.84	−0.34

Note: RMSE = root mean square error; MAE = mean absolute error; SEE = standard error of estimate; r = Pearson's correlation coefficient; LOOCV = leave-one-out cross-validation; CV = cross-validation; Bias = mean prediction error. AGB is expressed in Mg ha^{-1}. SEE and Pearson's r were calculated for calibration only, whereas bias was calculated from cross-validation predictions.

Figure 8 confirms the strong relationship between field-estimated AGB and predicted AGB for both NDVI- and SAVI-based models. The two models produced identical statistical performance, indicating that SAVI was highly collinear with NDVI in the present dataset. Therefore, the combined use of NDVI and SAVI was not retained in the final regression model. The NDVI-based model was selected as the most parsimonious model for spatial AGB estimation, while SAVI was considered a complementary soil-adjusted vegetation indicator.

The identical performance of NDVI and SAVI indicates that SAVI did not provide additional independent information compared with NDVI in the present dataset. Although SAVI is theoretically useful in open-canopy and semi-arid environments because it reduces soil-background effects, its added value becomes limited when it is highly collinear with NDVI [12]. Therefore, the combined use of NDVI and SAVI in the same regression model should be avoided or interpreted cautiously, because collinearity may produce unstable regression coefficients without improving predictive performance [11].

The elevation-only model showed a weaker relationship with AGB, explaining 17.6% of biomass variability, with RMSE = 95.04 Mg ha^{-1}. When elevation was added to NDVI or SAVI, model performance improved only slightly, with R^2 increasing from 0.783 to 0.784 and RMSE decreasing from 48.77 to 48.65 Mg ha^{-1}. This very small improvement indicates that elevation contributed limited additional predictive information once vegetation greenness was already included in the model. Nevertheless, elevation remains ecologically meaningful in the Ouled Yagoub Forest because *Cedrus atlantica* is more frequent in higher and relatively humid sectors, whereas *Pinus halepensis* is more common at lower elevations and degraded slopes. El Mderssa et al., [17] also reported that Atlas cedar is mainly associated with mountainous zones, confirming the ecological importance of altitude for cedar distribution.

The combined NDVI + SAVI + elevation model also reached R^2 = 0.784 and RMSE = 48.65 Mg ha^{-1}. However, this model was not retained as the final model because NDVI and SAVI were highly collinear and did not improve predictive performance [23]. Therefore, the NDVI-based model was considered the most parsimonious model for spatial AGB estimation, while elevation was retained mainly as an ecological variable supporting the interpretation of biomass distribution along the altitudinal gradient. This approach follows the principle that empirical biomass models should balance predictive performance, ecological interpretability, and model simplicity [31].

These results indicate that canopy greenness is a strong indicator of above-ground biomass variability in the Ouled Yagoub Forest. Higher NDVI values were generally associated with denser and structurally developed forest patches, whereas lower values corresponded to sparse vegetation, degraded stands, open-canopy areas, or zones affected by disturbance. However, biomass and carbon storage should not be interpreted only as spectral responses. Forest carbon dynamics are also influenced by climatic variability, drought, fire, disturbance history, and ecosystem physiological responses. Niu et al. [4] emphasized that interannual variability in terrestrial carbon exchange is driven by climate anomalies and their effects on photosynthesis and respiration, with semi-arid ecosystems playing an important role in land carbon variability (Figure 8).

The limited contribution of elevation suggests that altitude alone cannot fully explain biomass patterns, although it remains ecologically relevant because *Cedrus atlantica* is more frequent in higher and relatively humid sectors of the massif [23]. In the present field inventory, healthy *Cedrus atlantica* trees showed much higher mean AGB per tree than declining cedar and *Pinus halepensis*, confirming the strong contribution of cedar-dominated stands to biomass storage. This supports the interpretation that biomass distribution is controlled not only by canopy greenness, but also by species composition, tree size, stand structure, and tree health status. The use of species-specific allometric equations is therefore important for improving biomass estimation in mixed forest stands [17].

Overall, the results show that Sentinel-2 vegetation indices can support biomass estimation when calibrated with field inventory data. Nevertheless, the collinearity between NDVI and SAVI indicates that both indices should not be used together in the same final regression model. Future modelling should integrate independent predictors such as Sentinel-2 red-edge indices, EVI, canopy height, forest type, slope, aspect, texture variables,

fire history, and cedar health status to improve model robustness and reduce uncertainty in biomass and carbon-stock mapping. This recommendation is consistent with [4], who emphasized the need to combine observations, modelling frameworks, and statistical approaches to improve carbon-cycle prediction (Table 8 and Figure 8).

Table 8. Pearson correlation matrix among field AGB, vegetation indices and elevation.

Variable	AGB	NDVI	SAVI	Elevation
AGB	1.000	0.885	0.885	0.420
NDVI	0.885	1.000	1.000	0.506
SAVI	0.885	1.000	1.000	0.506
Elevation	0.420	0.506	0.506	1.000

Carbon-stock estimation also depends on the reliability of biomass-to-carbon conversion parameters. For *Cedrus atlantica*, a measured carbon fraction of 0.5643 tC tMS^{-1} was reported, which is higher than the generic IPCC value of 0.51 tC tMS^{-1}. This confirms the importance of using species-specific carbon parameters for Atlas cedar carbon accounting, especially in Mediterranean mountain forests where generic conversion factors may introduce uncertainty into carbon-stock estimates [17].

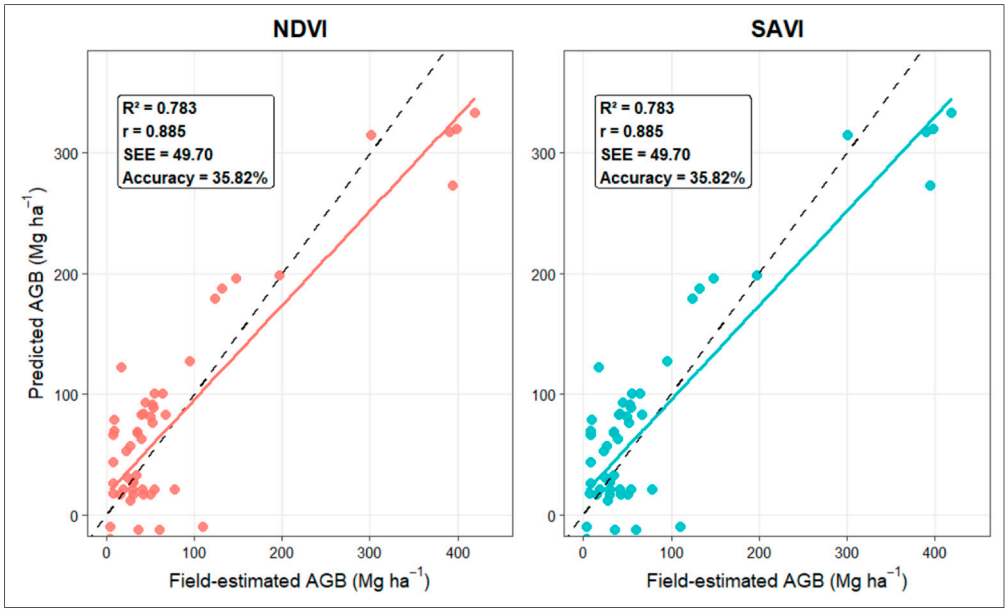


Figure 8. Relationship between field-estimated and predicted above-ground biomass (AGB) using NDVI- and SAVI-based models. The solid lines represent the fitted regression lines, the dashed lines represent the 1:1 reference lines, and the symbols represent the observed data points.

The NDVI model was retained as the most parsimonious model because it provided strong predictive performance while avoiding collinearity problems associated with the simultaneous use of NDVI and SAVI [11].

Although NDVI explained a high proportion of AGB variability, the model remains empirical and field-calibrated. Therefore, its transferability to other forests or acquisition dates should be tested carefully, especially because semi-arid ecosystems are sensitive to interannual climate variability, drought, fire, and disturbance effects on carbon exchange [4].

Relationship Between AGB and Environmental Predictors

Linear regression analysis was performed to evaluate the relationship between field-estimated above-ground biomass (AGB) and the explanatory variables derived from Sentinel-2 imagery and topography. The integration of remote sensing data with geospatial techniques has proven effective for assessing land resources and vegetation patterns in semi-arid regions [32]. The results showed a strong and highly significant positive relationship between AGB and both vegetation indices. NDVI explained 78.3% of the spatial variation in AGB, with a Pearson correlation coefficient of r = 0.885. SAVI showed a similar performance, with R^2 = 0.783 and r = 0.885, confirming the relevance of Sentinel-2 vegetation indices for biomass estimation in the Ouled Yagoub Forest (Table 9). Similar results have been reported in other semi-arid forest ecosystems; for instance, Torabzadeh et al. [33] found that Sentinel-2 data explained 87% of AGB variability in the Zagros Forest, Iran (R^2 = 0.87, RMSE = 10.75 t ha^{-1}).

Table 9. Performance of AGB regression models using spectral and topographic predictors.

Model	R^2	RMSE Mg ha^{-1}	Interpretation
AGB~NDVI	0.783	48.77	Strong relationship
AGB~SAVI	0.783	48.77	Strong relationship, but redundant with NDVI
AGB~Elevation	0.176	95.04	Weak to moderate relationship
AGB~NDVI + Elevation	0.784	48.65	Very small improvement compared with NDVI alone
AGB~SAVI + Elevation	0.784	48.65	Very small improvement compared with SAVI alone
AGB~NDVI + SAVI + Elevation	0.784	48.65	Collinearity issue; not retained as final model

In contrast, altitude showed a weaker but statistically significant relationship with AGB, explaining only 17.6% of the variation. This indicates that vegetation greenness and canopy density are stronger predictors of above-ground biomass than elevation alone (Figure 5). This result agrees with the outcomes of Chakroun et al. [34], who showed that NDVI and related vegetation indices are better than SAVI for biomass-related assessments in Mediterranean forest ecosystems.

The strong relationships observed for NDVI and SAVI suggest that forest biomass in the study area is closely related to vegetation vigour and canopy cover. Similar findings have also been reported in Mediterranean forests of southern Spain, where NDVI and tree density positively affected forest biomass and productivity strongly for several species such as *Pinus halepensis* and *Quercus ilex* [35] (Figure 9).

Higher AGB values were generally associated with higher vegetation index values, corresponding to denser and more productive forest stands. The weaker relationship with altitude suggests that elevation may influence biomass indirectly through species distribution, stand structure, soil conditions, and microclimatic gradients, but it is not sufficient as a single predictor for biomass modelling. This is consistent with recent results from Mediterranean semi-arid forests, where the effect of canopy cover on aboveground biomass was the strongest direct effect (β = 0.36), while the effect of elevation on biomass was indirect through its effect on canopy cover, structural diversity and species composition [36]. Similarly, Di Biase et al. [37] showed that in Mediterranean mountain ecosystems species composition and vegetation structure varied systematically along elevational gradients, with a decrease in Mediterranean species and an increase in species adapted to high altitude with elevation, which in turn influences patterns of biomass accumulation.

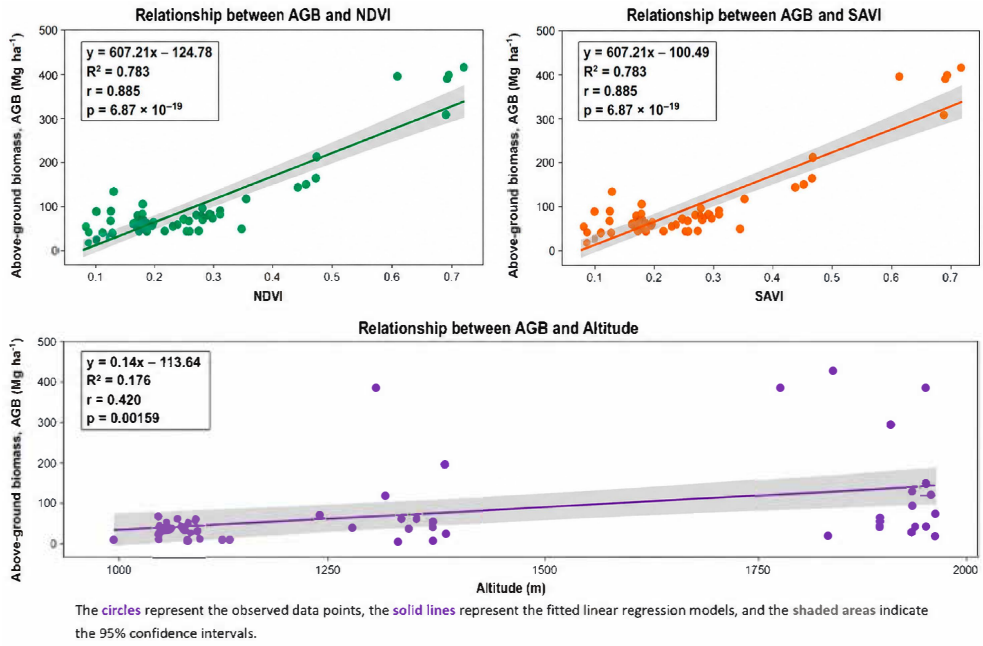


Figure 9. Relationships between field-estimated above-ground biomass (AGB) and Sentinel-2 vegetation indices NDVI and SAVI, and altitude in the Ouled Yagoub Forest. The regression line represents the fitted linear model, while R^2, Pearson's correlation coefficient (r), and *p*-value indicate the strength and statistical significance of each relationship.

3.4. Spatial Estimation of AGB Using the Selected NDVI Model

The selected NDVI-based model was applied to the Sentinel-2 NDVI raster to generate a spatial estimate of AGB across the Ouled Yagoub Forest. These maps should be interpreted as field-calibrated exploratory spatial estimates rather than independently validated carbon maps. They represent the spatial application of the retained NDVI-based regression model and are therefore dependent on the field dataset, allometric equations, Sentinel-2 spectral response and model uncertainty. This model was retained because it provided strong predictive performance while avoiding collinearity problems associated with the combined use of NDVI and SAVI. This approach is in line with recent studies in Mediterranean forest ecosystems that have shown that optical imagery from Sentinel-2 is more effective than radar-based models for estimating forest structure and aboveground biomass [38].

Higher estimated AGB values were mainly associated with dense and structurally developed forest patches, particularly cedar-dominated stands, whereas lower values corresponded to sparse pine formations, open-canopy areas, degraded stands, or disturbed zones. Other forest ecosystems have also reported similar patterns, with higher NDVI values representing denser vegetation cover and higher biomass accumulation, and lower values representing sparse or degraded vegetation [39]. According to Chen et al. [40], high biomass patches are always associated with higher canopy density and well-developed stand structure, while low biomass patches are usually associated with open canopies and degraded vegetation conditions.

The NDVI-based AGB map shows a heterogeneous spatial distribution of above-ground biomass across the Ouled Yagoub Forest. Very high and high AGB classes are mainly concentrated in the central and northeastern parts of the study area, where dense and structurally developed forest patches are more frequent. These areas likely correspond to better-developed stands, including cedar-dominated formations and dense mixed forest patches. In contrast, very low and low AGB classes occur mainly in open-canopy, degraded, or sparsely vegetated areas, particularly in peripheral and lower-density forest zones. This spatial pattern confirms the strong structural heterogeneity of the Ouled Yagoub Forest

and reflects the combined influence of vegetation density, species composition, disturbance history, and ecological gradients on biomass distribution (Figure 10).

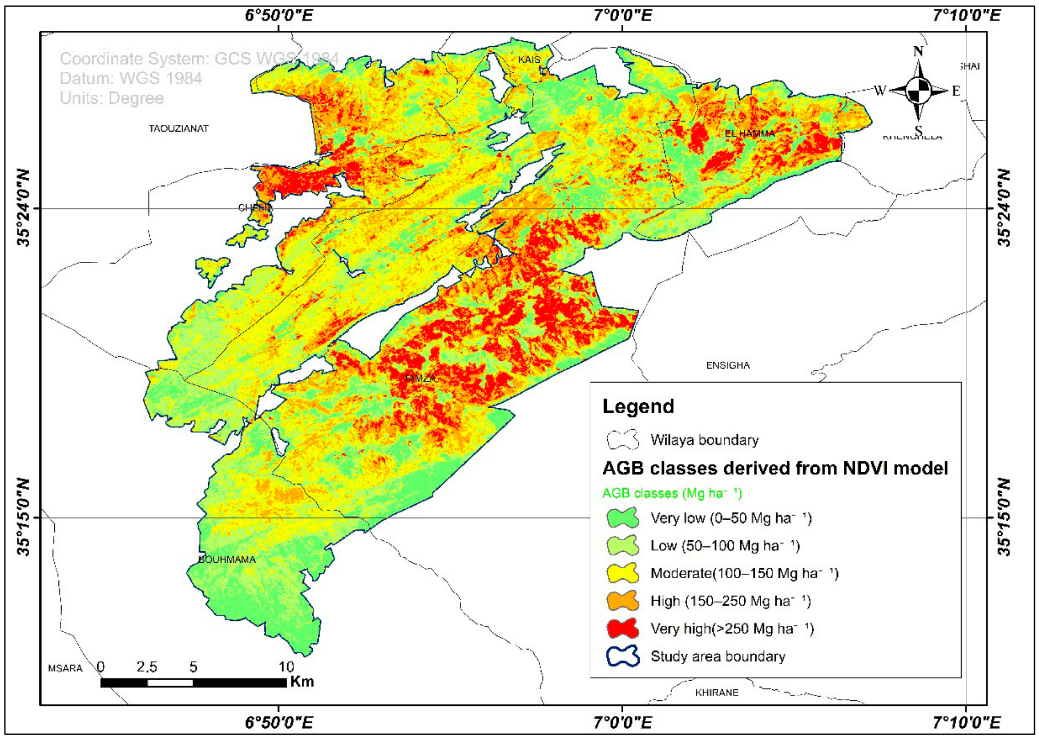


Figure 10. Spatial distribution of above-ground biomass estimated using the selected NDVI-based model.

3.5. Carbon Stock and CO_2-Equivalent Estimation

Applying the carbon conversion chain described in Section 2.6 to the field-estimated AGB values and to the NDVI-based spatial AGB model, the carbon accounting results summarized in Figure 11 were obtained. Figure 11 summarizes the biomass, carbon stock, and CO_2-equivalent storage estimated from the field inventory in the Ouled Yagoub Forest. The total above-ground biomass reached 338.07 Mg, while total biomass, including below-ground biomass, reached 436.11 Mg. The corresponding carbon stock was 238.56 Mg C, equivalent to 874.78 Mg CO_2eq. At the hectare scale, these values corresponded to 62.61 Mg ha^{-1} for AGB, 80.76 Mg ha^{-1} for total biomass, 44.18 Mg C ha^{-1} for carbon stock, and 162.00 Mg CO_2eq ha^{-1} for CO_2-equivalent storage. These values are consistent with the carbon accounting results presented in Table 8.

Figure 11 clearly shows the dominant contribution of *Cedrus atlantica* to biomass and carbon storage. Although *Pinus halepensis* was numerically more abundant in the field inventory, *Cedrus atlantica* contributed 247.14 Mg of AGB, compared with 90.93 Mg for *P. halepensis*. This represents approximately 73.1% of total AGB. The same dominance is observed for total biomass, carbon stock, and CO_2-equivalent storage. This pattern reflects the larger stem diameter and higher individual biomass of cedar trees, especially healthy cedar individuals. Comparative studies in Mediterranean forest ecosystems have shown that different ecological behaviours were observed for *Cedrus atlantica* and *Pinus halepensis*, with *Pinus halepensis* tending to produce higher metabolic quotients in soil microbial biomass, while *Cedrus atlantica* is related to different organic matter dynamics and carbon cycling patterns [41].

The field inventory estimated a total AGB of 338.07 Mg, corresponding to 62.61 Mg ha^{-1}. After below-ground biomass expansion, total biomass reached 436.11 Mg, equivalent to 80.76 Mg ha^{-1}. The total carbon stock was estimated at 238.56 Mg C, correspond-

ing to 44.18 Mg C ha^{-1}, while CO_2-equivalent storage reached 874.78 Mg CO_2eq, or 162.00 Mg CO_2eq ha^{-1}.

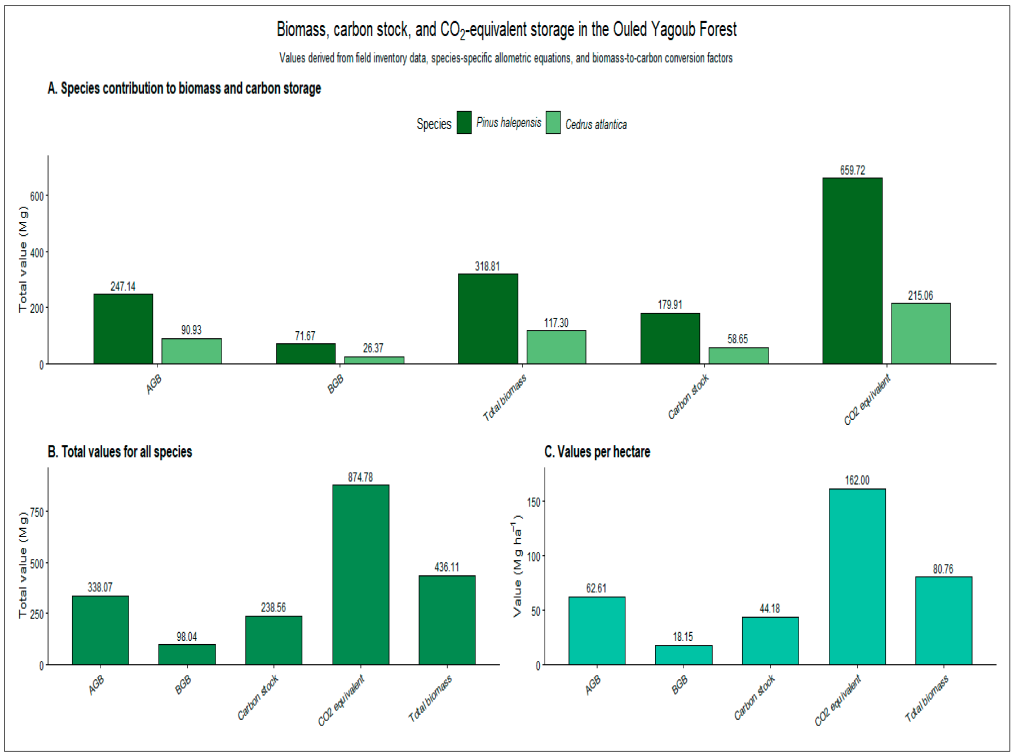


Figure 11. Biomass, carbon stock, and CO_2-equivalent storage in the Ouled Yagoub Forest. (**A**) Species contribution to above-ground biomass, below-ground biomass, total biomass, carbon stock, and CO_2-equivalent storage; (**B**) total values for all species; and (**C**) values expressed per hectare. Values were derived from field inventory data, species-specific allometric equations, and biomass-to-carbon conversion factors. *Cedrus atlantica* contributed the largest share of biomass and carbon storage despite being less abundant than *Pinus halepensis*. Note: FC = 0.50 for *P. halepensis*; FC = 0.5643 for *C. atlantica* following [17] root-to-shoot ratio = 0.29; CO_2eq = C × 3.667.

The mean AGB value obtained in this study, 62.61 Mg ha^{-1}, is comparable to values reported for some Mediterranean forest stands. For example, Boulmane et al. [42] reported AGB values of approximately 58–64 Mg ha^{-1} for *Quercus ilex* stands in the Moroccan Middle Atlas [42]. In terms of carbon stock, the value obtained in the present study, 44.18 Mg C ha^{-1}, remains lower than the 78.75 Mg C ha^{-1} reported by El Mderssa et al., [17] for mature Atlas cedar stands, but it falls within the range of 40–77 Mg C ha^{-1} reported by [43] for degraded cork oak forests in Morocco. This intermediate value reflects the mixed and heterogeneous structure of the Ouled Yagoub Forest, which includes young pine formations, open-canopy stands, degraded patches, and mature cedar-dominated areas (Figure 11).

The contribution of *Cedrus atlantica* to carbon storage was dominant. Although cedar trees were less abundant than *Pinus halepensis*, they contributed 247.14 Mg of AGB, representing 73.1% of the total AGB. This confirms the key role of large cedar individuals in maintaining the biomass and carbon-storage capacity of the forest.

Declining *Cedrus atlantica* individuals showed lower estimated biomass and carbon storage than healthy cedar individuals. However, this result should be interpreted as an observed difference in estimated biomass and carbon storage, not as a direct causal quantification of carbon loss due to dieback. Tree size, age, stand density, site quality and disturbance history may also influence biomass differences between healthy and declining trees. In addition, the same allometric equation was applied to healthy and declining cedar trees because no specific equation is currently available for declining *Cedrus atlantica*. This

may overestimate biomass in declining individuals affected by crown dieback, branch loss or reduced foliage density. Therefore, the carbon-loss estimate should be considered indicative and should be refined in future studies using crown-condition measurements and health-specific allometric models (Figure 11).

The spatial carbon-stock and CO_2-equivalent maps were derived from the NDVI-based AGB map using the biomass-to-carbon conversion chain described in Section 2.6. Therefore, their spatial patterns closely follow the distribution of predicted AGB. Higher carbon-stock and CO_2-equivalent values are mainly associated with dense and structurally developed forest patches, whereas lower values occur in sparse, degraded, or open-canopy areas.

High carbon-stock classes indicate areas with higher predicted biomass and denser vegetation cover, but they should not be interpreted as direct indicators of severe mortality or cedar dieback. Conversely, low carbon-stock classes may correspond to open canopy, degraded vegetation, burned areas, sparse stands or naturally low-density forest conditions.

The carbon-stock map shows a heterogeneous spatial distribution across the Ouled Yagoub Forest. High carbon-stock values, ranging from 75 to 98.5 Mg C ha^{-1}, are mainly concentrated in the central, northern, and northeastern parts of the study area. These zones correspond to dense and structurally developed forest patches, where high above-ground biomass is expected. In contrast, very low and low carbon-stock classes are mainly distributed in open-canopy, sparse, or degraded areas, particularly in peripheral sectors and lower-density forest formations.

This spatial pattern reflects the strong dependence of carbon storage on forest structure and biomass density. Since the carbon-stock map was derived from the NDVI-based AGB model, areas with high NDVI and high predicted AGB also show higher carbon-stock values. Therefore, the map should be interpreted as a spatial estimate of living biomass carbon rather than a direct measurement of carbon content (Figure 12).

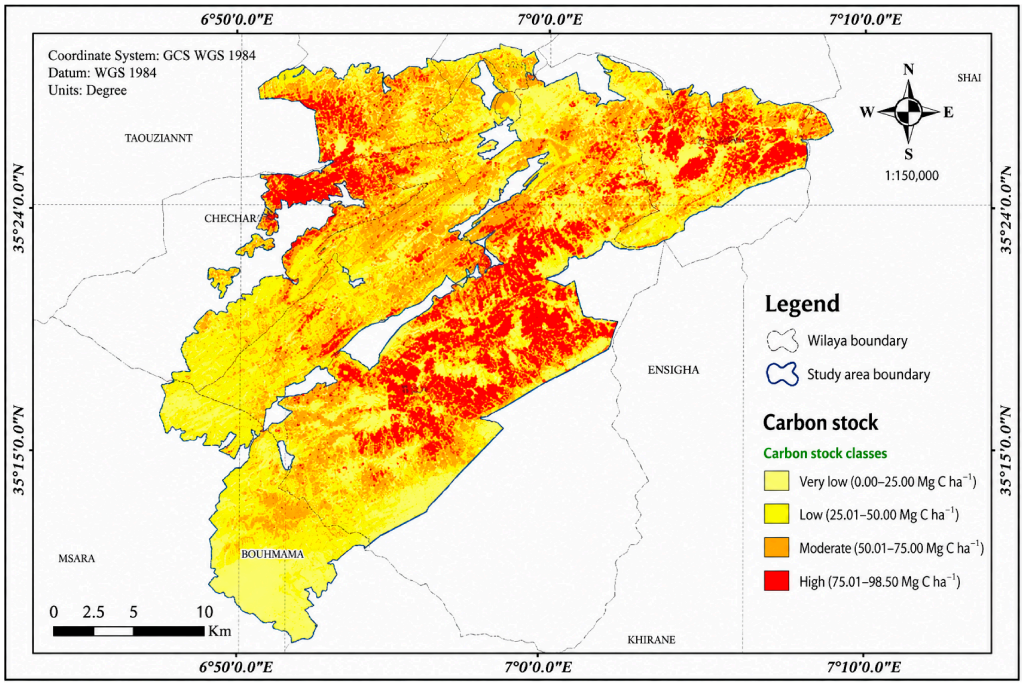


Figure 12. Spatial distribution of carbon stock derived from the NDVI-based AGB model.

The CO_2-equivalent storage map follows the same spatial pattern as the carbon-stock map because it was directly derived from carbon stock using the molecular conversion factor of 3.667. High CO_2-equivalent values, ranging from 270 to 361 Mg CO_2eq ha^{-1}, are concentrated in the same dense forest sectors that showed high carbon-stock values. These

areas represent the most important zones for climate-regulation services within the Ouled Yagoub Forest (Figure 13).

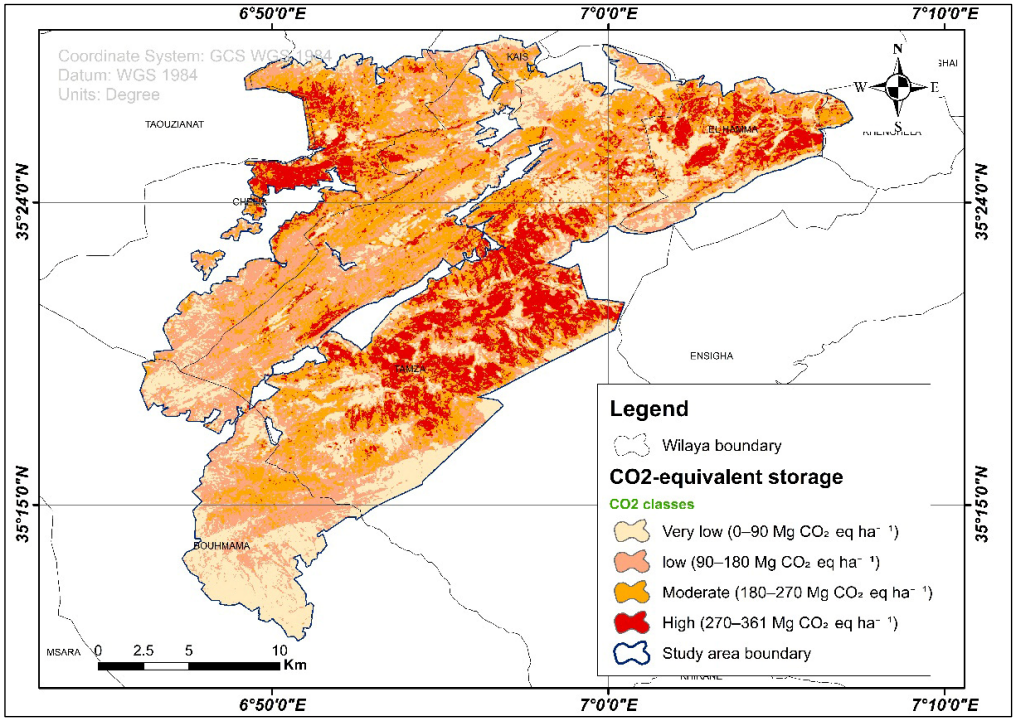


Figure 13. Spatial distribution of CO_2-equivalent storage derived from the NDVI-based carbon-stock model.

Lower CO_2-equivalent storage values occur in sparse, degraded, or open-canopy areas, where predicted AGB and carbon stock are reduced. This confirms that the climate-mitigation potential of the forest is spatially uneven and strongly linked to the conservation of dense and structurally developed stands. The highest carbon-stock and CO_2-equivalent classes are likely associated with dense and structurally developed forest patches, particularly cedar-dominated or mixed cedar stands, because *Cedrus atlantica* individuals stored much higher biomass per tree than *Pinus halepensis*. In the field inventory, healthy cedar trees showed substantially higher above-ground biomass than declining cedar trees, indicating that cedar health status directly influences carbon-storage capacity. The inventory included 661 measured trees, with 467 *Pinus halepensis* and 194 *Cedrus atlantica* individuals, including 122 healthy and 72 declining cedar trees [5].

These high carbon-stock zones should therefore be considered priority areas for cedar conservation. If dense cedar-dominated sectors are progressively affected by dieback, they may experience future carbon losses through reduced radial growth, branch mortality, tree mortality, and subsequent biomass decomposition [7]. This interpretation is consistent with studies reporting that Atlas cedar decline is associated with drought stress, aridification, growth reduction, and biotic damage, including bark beetle and woodborer outbreaks in the Aurès region [6].

The red/high classes on the carbon-stock and CO_2-equivalent maps should not be interpreted as direct indicators of severe dieback. They represent areas with high estimated biomass and carbon storage derived from the NDVI-based AGB model. To identify where cedar dieback represents the greatest threat to forest carbon stocks, future analyses should overlay the carbon-stock map with a cedar health-status or dieback-severity map [44]. The most critical zones would correspond to areas where high carbon-stock values coincide with declining cedar stands. This integrated approach is recommended because recent

biomass-mapping studies emphasize the value of combining spectral information with structural, ecological and disturbance-related variables to reduce uncertainty in forest carbon-stock assessment [9].

3.6. Model Uncertainty and Limitations

The performance of the NDVI- and SAVI-based AGB models was evaluated using SEE, RMSE, MAE, Pearson's correlation coefficient, and the coefficient of determination. In addition, SEE-based relative accuracy was calculated following the approach of [45] (Equation (13)).

$$Accuracy(\%) = \left(1 - \frac{SEE}{\bar{AGB}_{field}}\right) \times 100 \quad (13)$$

where SEE is the standard error of the estimate and mean field-estimated AGB corresponds to the average plot-level AGB used for model calibration. The results are summarized in Table 10.

Table 10. Regression performance, error metrics, and SEE-based relative accuracy of NDVI- and SAVI-based above-ground biomass models.

Model	Regression Equation	n	Mean Field AGB (Mg ha^{-1})	SEE (Mg ha^{-1})	RMSE (Mg ha^{-1})	MAE (Mg ha^{-1})	Pearson (r)	R^2	SEE-Based Relative Accuracy (%)
NDVI-based AGB model	AGB = 607.21 × NDVI − 124.78	54	62.61	49.70	48.77	39.14	0.885	0.783	35.82
SAVI-based AGB model	AGB = 607.21 × SAVI − 100.49	54	62.61	49.70	48.77	39.14	0.885	0.783	35.82

This comparison will determine the most accurate vegetation index for AGB estimation in the Ouled Yagoub Forest, and will directly confirm whether SAVI's soil-adjustment advantage is significant in the semi-arid pine zone as it was in the mangrove context [45].

Although the NDVI-based model explained a high proportion of AGB variability, the SEE and RMSE values indicate that substantial prediction uncertainty remains. This uncertainty is likely related to the structural heterogeneity of the Ouled Yagoub Forest, including variation in species composition, tree size, stand density, canopy closure, cedar health status, topographic position, and disturbance history. Similar limitations have been reported in Sentinel-2-based AGB studies, where simple optical vegetation indices may be affected by canopy saturation, topographic complexity, and the limited ability of spectral variables to represent forest vertical structure [8,9].

Future biomass modelling should therefore integrate additional and more independent predictors. Sentinel-2 red-edge bands, enhanced vegetation indices, and texture metrics have shown strong sensitivity to forest AGB and can reduce overestimation and underestimation errors [46]. In addition, combining Sentinel-2 optical data with Sentinel-1 SAR can improve biomass estimation because radar backscatter provides complementary structural information that is not fully captured by optical indices [47]. For higher-biomass and structurally complex stands, LiDAR-derived canopy height and vertical-structure metrics are particularly valuable because they help reduce saturation effects and improve biomass prediction accuracy [48].

Therefore, the spatial AGB, carbon-stock, and CO_2-equivalent maps produced in this study should be interpreted as field-calibrated spatial estimates rather than direct measurements of forest carbon stock. Future work should include independent validation plots or cross-validation procedures, together with Sentinel-2 red-edge indices, EVI, NDMI, NBR, texture variables, Sentinel-1 SAR features, LiDAR-derived canopy height, slope, aspect, forest type, fire history, and cedar health-status indicators. Such an integrated

approach would improve model robustness and reduce uncertainty in biomass and carbon-stock mapping in semi-arid Mediterranean mountain forests.

4. Limitations and Future Research

This study has several limitations. First, the spatial models relied on 54 stocked plots, and the analysis did not include a fully independent external validation dataset. Although LOOCV and 5-fold cross-validation evaluated model stability, future research should include independent validation plots distributed across forest types, elevation classes and disturbance gradients. Second, the primary stocked-plot calibration excluded six treeless or severely degraded plots, which may lead to AGB overestimation in low-biomass areas. Third, the use of the same allometric equation for healthy and declining cedar trees may overestimate biomass in individuals affected by crown dieback or branch loss. Fourth, the study estimated carbon stock from biomass conversion factors rather than from direct carbon-concentration measurements for all tree components. Future studies should integrate Sentinel-2 red-edge indices, EVI, NDMI, NBR, texture variables, Sentinel-1 SAR features, UAV or LiDAR-derived canopy height, forest-type maps, fire-history layers and larger validation datasets to improve biomass and carbon-stock mapping.

5. Conclusions

This study provides a field-calibrated assessment of AGB, total biomass, carbon stock and CO_2-equivalent storage in the Ouled Yagoub Forest, northeastern Algeria. Based on 661 measured trees distributed across 54 stocked circular plots, field-estimated AGB reached 338.07 Mg, corresponding to 62.61 Mg ha^{-1} for stocked plots. Total biomass reached 436.11 Mg after below-ground biomass expansion, while carbon stock and CO_2-equivalent storage reached 238.56 Mg C and 874.78 Mg CO_2eq, respectively. *Cedrus atlantica* contributed the largest share of biomass and carbon storage in the sampled stands, mainly because cedar trees had larger stem diameters and higher individual biomass than *Pinus halepensis*. Declining *Cedrus atlantica* individuals showed lower estimated biomass and carbon storage than healthy cedar individuals, but this difference should be interpreted as an observed pattern rather than a direct causal estimate of carbon loss due to dieback.

The NDVI-based model showed good calibration performance and acceptable cross-validation stability. The model explained 78.3% of AGB variability during calibration, with Pearson's r = 0.885, RMSE = 48.77 Mg ha^{-1} and MAE = 39.14 Mg ha^{-1}. Cross-validation results remained close to the calibration statistics, with LOOCV R^2 = 0.755 and RMSE = 51.86 Mg ha^{-1}, and 5-fold CV R^2 = 0.762 and RMSE = 51.07 Mg ha^{-1}. SAVI produced identical predictive performance because it was perfectly collinear with NDVI in the plot dataset and therefore did not provide additional independent information. Elevation alone showed weaker predictive performance, and its combination with NDVI produced only a marginal calibration improvement without improving cross-validated performance. Consequently, the NDVI-only model was retained as the most parsimonious model for spatial AGB prediction, while elevation was retained mainly for ecological interpretation along the altitudinal gradient.

The spatial AGB, carbon-stock and CO_2-equivalent maps derived in this study provide useful field-calibrated exploratory spatial estimates for forest carbon monitoring in the Aurès Mountains. However, these outputs should not be interpreted as direct measurements or independently validated carbon maps. They remain dependent on the field dataset, plot representativeness, allometric equations, biomass-to-carbon conversion factors, Sentinel-2 spectral response, model uncertainty and the exclusion of treeless or severely degraded plots from the primary stocked-plot calibration. High carbon-stock classes indicate areas with higher predicted biomass and denser vegetation cover, but they should not

be interpreted as direct indicators of severe mortality or cedar dieback. Conversely, low carbon-stock classes may correspond to open canopy, degraded vegetation, burned areas, sparse stands or naturally low-density forest conditions.

Future work should integrate independent validation plots, larger sampling across forest types and disturbance gradients, direct carbon-content measurements, crown-condition measurements, health-specific allometric models for declining *Cedrus atlantica*, Sentinel-2 red-edge indices, EVI, NDMI, NBR, texture variables, Sentinel-1 SAR data, UAV or LiDAR-derived canopy-height metrics, fire-history layers and forest-type maps. Such an integrated approach would improve model robustness, reduce uncertainty and support climate-smart forest management, cedar conservation and restoration planning in the Ouled Yagoub Forest and comparable semi-arid Mediterranean mountain ecosystems.

Author Contributions: Conceptualization, O.M., T.A., Y.B. and A.S.A.; Methodology, O.M., T.A., Y.B. and M.S.S.; Software, O.M., T.A. and Y.B.; Validation, O.M.; Formal analysis, O.M., T.A., Y.B., A.S.A. and M.S.S.; Investigation, O.M., T.A., Y.B. and M.S.S.; Resources, O.M. and Y.B.; Data curation, O.M.; Writing—original draft, O.M., T.A., Y.B. and M.S.S.; Writing—review & editing, O.M., Y.B., A.S.A. and M.S.S.; Visualization, O.M. and Y.B.; Supervision, T.A. All authors have read and agreed to the published version of the manuscript.

Funding: This research received no external funding.

Institutional Review Board Statement: Not applicable.

Informed Consent Statement: Not applicable.

Data Availability Statement: The original contributions presented in this study are included in the article. Further inquiries can be directed to the corresponding author.

Acknowledgments: This publication has been supported by the RUDN University.

Conflicts of Interest: The authors declare no conflicts of interest.

References

1. Calvo Buendia, E.; Tanabe, K.; Kranjc, A.; Baasansuren, J.; Fukuda, M.; Ngarize, S.; Osako, A.; Pyrozhenko, Y.; Shermanau, P.; Federici, S. *2019 Refinement to the 2006 IPCC Guidelines for National Greenhouse Gas Inventories*; IPCC: Geneva, Switzerland, 2019.
2. Intergovernmental Panel on Climate Change. *2006 IPCC Guidelines for National Greenhouse Gas Inventories*; Institute for Global Environmental Strategies: Yokohama, Japan, 2006.
3. Friedlingstein, P.; O'Sullivan, M.; Jones, M.W.; Andrew, R.M.; Hauck, J.; Landschützer, P.; Le Quéré, C.; Li, H.; Luijkx, I.T.; Olsen, A.; et al. Global Carbon Budget 2024. *Earth Syst. Sci. Data* **2025**, *17*, 965–1039. [CrossRef]
4. Niu, S.; Fu, Z.; Luo, Y.; Stoy, P.C.; Keenan, T.F.; Poulter, B.; Zhang, L.; Piao, S.; Zhou, X.; Zheng, H.; et al. Interannual variability of ecosystem carbon exchange: From observation to prediction. *Glob. Ecol. Biogeogr.* **2017**, *26*, 1225–1237. [CrossRef]
5. Camarero, J.J.; Sánchez-Salguero, R.; Sangüesa-Barreda, G.; Lechuga, V.; Viñegla, B.; Seco, J.I.; Taïqui, L.; Carreira, J.A.; Linares, J.C. Drought, axe and goats. More variable and synchronized growth forecasts worsening dieback in Moroccan Atlas cedar forests. *Sci. Total Environ.* **2021**, *765*, 142752. [CrossRef]
6. Sarmoum, M.; Camarero, J.J.; Abdoun, F. Aridification increases growth resistance of Atlas cedar forests in NW Algeria. *For. Ecol. Manag.* **2024**, *556*, 121730. [CrossRef]
7. Beghami, R.; Bertella, N.; Laamari, M.; Bensaci, O.A. Bark beetle and woodborer insects' outbreak as a potent driver of Atlas cedar (*Cedrus atlantica* (Endl.) Carriere) forests dieback in Aures-East Algeria. *For. Sci. Technol.* **2020**, *16*, 75–85. [CrossRef]
8. Zhang, X.; Shen, H.; Huang, T.; Wu, Y.; Guo, B.; Liu, Z.; Luo, H.; Tang, J.; Zhou, H.; Wang, L.; et al. Improved random forest algorithms for increasing the accuracy of forest aboveground biomass estimation using Sentinel-2 imagery. *Ecol. Indic.* **2024**, *159*, 111752. [CrossRef]
9. Liu, P.; Ren, C.; Yang, X.; Wang, Z.; Jia, M.; Zhao, C.; Yu, W.; Ren, H. Combining Sentinel-2 and diverse environmental data largely improved aboveground biomass estimation in China's boreal forests. *Sci. Rep.* **2024**, *14*, 27528. [CrossRef]
10. Muhammad, B.; Rehman, A.U.; Mumtaz, F.; Qun, Y.; Zhongkui, J. Estimation of above-ground biomass in dry temperate forests using Sentinel-2 data and random forest: A case study of the Swat area of Pakistan. *Front. Environ. Sci.* **2024**, *12*, 1448648. [CrossRef]

11. Tucker, C.J. Red and photographic infrared linear combinations for monitoring vegetation. *Remote Sens. Environ.* **1979**, *8*, 127–150. [CrossRef]
12. Huete, A.R. A soil-adjusted vegetation index (SAVI). *Remote Sens. Environ.* **1988**, *25*, 295–309. [CrossRef]
13. Li, L.; Zhou, B.; Liu, Y.; Wu, Y.; Tang, J.; Xu, W.; Wang, L.; Ou, G. Reduction in uncertainty in forest aboveground biomass estimation using Sentinel-2 images: A case study of *Pinus densata* forests in Shangri-La City, China. *Remote Sens.* **2023**, *15*, 559. [CrossRef]
14. Ispikoudis, S.; Zianis, D.; Tziolas, E.; Damianidis, C.; Rapti, D.; Tsiros, E.; Michalakis, D.; Karteris, A. Assessment of Forest Biomass and Carbon Storage in Habitat 9340 *Quercus ilex* L. to Support Management Decisions for Climate Change Mitigation. *Sustainability* **2024**, *16*, 1403. [CrossRef]
15. Song, J.; Liu, X.; Adingo, S.; Guo, Y.; Li, Q. A comparative analysis of remote sensing estimation of aboveground biomass in boreal forests using machine learning modeling and environmental data. *Sustainability* **2024**, *16*, 7232. [CrossRef]
16. Chen, Z.; Yang, X.; Pan, X.; Wu, T.; Lei, J.; Chen, X.; Li, Y.; Chen, Y. Estimating forest aboveground biomass in tropical zones by integrating LiDAR and Sentinel-2B data. *Sustainability* **2025**, *17*, 3631. [CrossRef]
17. El Mderssa, M.; Malki, F.; Ikraoun, H.; Nassiri, L.; Ibijbijen, J. Determining parameters to assess carbon stocks in forest ecosystems with *Cedrus atlantica* Manetti (Atlas Cedar) in Morocco: Specific and generic methods. *Bois For. Trop.* **2022**, *351*, 67–77.
18. CFK. *Rapport Technique sur la Forêt Domaniale D'Ouled Yagoub, Wilaya de Khenchela*; Conservation des Forêts de Khenchela: Khenchela, Algeria, 2023.
19. Meghithi, O.; Toufik, A.; Alturki, A.A.; Rebouh, N.Y.; Kholiyarov, E.; Ismoilov, M.; Abdeljawad, S.A.; Youssef, Y.M.; Shokr, M.S. Multi-index analysis for wildfire severity and vegetation dieback assessment in semi-arid forest ecosystems. *Front. For. Glob. Change* **2026**, *9*, 1809572. [CrossRef]
20. Mostafa, M.A.; Abuzaid, A.S.; El Ghonamey, Y.K.; Abbas, H.H. A GIS-based land suitability analysis in a newly reclaimed desert region of Egypt. *Ann. Agric. Sci. Moshtohor* **2025**, *63*, 178–188. [CrossRef]
21. Bentouati, A. Étude de la Cédraie de L'Aurès: Écologie, Structure et Dynamique des Peuplements de *Cedrus atlantica* Manetti. Master's thesis, Université de Batna, Batna, Algeria, 2006.
22. Chafai, C.; Bentouati, A.; Rabhi, K.; Sghaier, T.; Arar, A.; Bachir, A.S. Using GIS and AHP techniques to evaluate the forest site quality in the Ouled Yagoub National Forest (North-East, Algeria). *Genet. Biodivers. J.* **2023**, *7*, 94–108. [CrossRef]
23. Montero, G.; Ruiz-Peinado, R.; Munoz, M. *Producción de Biomasa y Fijación de CO_2 por los Bosques Españoles*; INIA: Madrid, Spain, 2011.
24. Gorelick, N.; Hancher, M.; Dixon, M.; Ilyushchenko, S.; Thau, D.; Moore, R. Google Earth Engine: Planetary-scale geospatial analysis for everyone. *Remote Sens. Environ.* **2017**, *202*, 18–27. [CrossRef]
25. Legesse, F.; Degefa, S.; Soromessa, T. Carbon stock dynamics in a changing land use land cover of the Upper Awash River Basin: Implications for climate change management. *Sustain. Environ.* **2024**, *10*, 2361565. [CrossRef]
26. Stone, M. Cross-validatory choice and assessment of statistical predictions. *J. R. Stat. Soc. B* **1974**, *36*, 111–147. [CrossRef]
27. Arlot, S.; Celisse, A. A survey of cross-validation procedures for model selection. *Stat. Surv.* **2010**, *4*, 40–79. [CrossRef]
28. Valbuena, R.; Hernando, A.; Manzanera, J.A.; Görgens, E.B.; Almeida, D.R.A.; Mauro, F.; García-Abril, A.; Coomes, D.A. Enhancing of accuracy assessment for forest above-ground biomass estimates obtained from remote sensing via hypothesis testing and overfitting evaluation. *Ecol. Model.* **2017**, *366*, 15–26. [CrossRef]
29. O'brien, K.; Eriksen, S.; Nygaard, L.P.; Schjolden, A.N.E. Why different interpretations of vulnerability matter in climate change discourses. *Clim. Policy* **2007**, *7*, 73–88. [CrossRef]
30. Thompson, C.G.; Kim, R.S.; Aloe, A.M.; Becker, B.J. Extracting the variance inflation factor and other multicollinearity diagnostics from typical regression results. *Basic Appl. Soc. Psychol.* **2017**, *39*, 81–90. [CrossRef]
31. Picard, N.; Saint-André, L.; Henry, M. *Manual for Building Tree Volume and Biomass Allometric Equations: From Field Measurement to Prediction*; FAO: Rome, Italy, 2012.
32. Mostafa, M.A.; Abuzaid, A.S.; El Ghonamey, Y.K.; Abbas, H.H. Land resources assessment in western Nile Delta of Egypt using geospatial techniques. *Ann. Agric. Sci. Moshtohor* **2025**, *63*, 167–177. [CrossRef]
33. Torabzadeh, H.; Moradi, M.; Fatehi, P. Estimating aboveground biomass in zagros forest, Iran, using sentinel-2 data. *Int. Arch. Photogramm. Remote Sens. Spat. Inf. Sci.* **2019**, *42*, 1059–1063. [CrossRef]
34. Chakroun, H.; Mouillot, F.; Hamdi, A. Regional equivalent water thickness modeling from remote sensing across a tree cover/LAI gradient in Mediterranean forests of Northern Tunisia. *Remote Sens.* **2015**, *7*, 1937–1961. [CrossRef]
35. Herraiz, A.D.; Salazar-Zarzosa, P.C.; Mesas, F.J.; Arenas-Castro, S.; Ruiz-Benito, P.; Villar, R. Modelling aboveground biomass and productivity and the impact of climate change in Mediterranean forests of South Spain. *Agric. For. Meteorol.* **2023**, *337*, 109498. [CrossRef]
36. Pordel, N.; Hosseinzadeh, J.; Heydari, M.; Omidipour, R. Structural relationships among topography, canopy cover, ecosystem functions, and soil quality in the semi-arid forests of the Zagros mountains. *For. Ecol. Manag.* **2026**, *601*, 123334. [CrossRef]
37. Di Biase, L.; Pace, L.; Mantoni, C.; Fattorini, S. Variations in plant richness, biogeographical composition, and life forms along an elevational gradient in a Mediterranean mountain. *Plants* **2021**, *10*, 2090. [CrossRef] [PubMed]

38. Mihai, M.C.; Miguel, S.; Borlaf-Mena, I.; Tijerín-Triviño, J.; Tanase, M. Assessing Forest Structure and Biomass with Multi-Sensor Remote Sensing: Insights from Mediterranean and Temperate Forests. *Forests* **2025**, *16*, 1164. [CrossRef]
39. Guerra-Hernández, J.; Narine, L.L.; Pascual, A.; Gonzalez-Ferreiro, E.; Botequim, B.; Malambo, L.; Neuenschwander, A.; Popescu, S.C.; Godinho, S. Aboveground biomass mapping by integrating ICESat-2, SENTINEL-1, SENTINEL-2, ALOS2/PALSAR2, and topographic information in Mediterranean forests. *GISci. Remote Sens.* **2022**, *59*, 1509–1533. [CrossRef]
40. Chen, J.; Song, B.; Rudnicki, M.; Moeur, M.; Bible, K.; North, M.; Shaw, D.C.; Franklin, J.F.; Braun, D.M. Spatial relationship of biomass and species distribution in an old-growth Pseudotsuga-Tsuga forest. *For. Sci.* **2004**, *50*, 364–375. [CrossRef]
41. Pinzari, F.; Dell'Abate, M.; Benedetti, A.; Dazzi, C. Effects of *Cedrus atlantica* and *Pinus halepensis* on the chemistry and fertility of a Mediterranean soil after 40 years. *Can. J. Soil Sci.* **2001**, *81*, 553–560. [CrossRef]
42. Boulmane, M.; Makhloufi, M.; Bouillet, J.-P.; Saint-André, L.; Satrani, B.; Halim, M.; Elantry-Tazi, S. Estimation du stock de carbone organique dans la chênaie verte du Moyen Atlas marocain. *Acta Bot. Gall.* **2010**, *157*, 451–467. [CrossRef]
43. Oubrahim, H.; Boulmane, M.; Bakker, M.R.; Augusto, L.; Halim, M. Carbon storage in degraded cork oak (*Quercus suber*) forests on flat lowlands in Morocco. *iForest—Biogeosci. For.* **2015**, *9*, 125. [CrossRef]
44. Ehlers, D.; Wang, C.; Coulston, J.; Zhang, Y.; Pavelsky, T.; Frankenberg, E.; Woodcock, C.; Song, C. Mapping forest aboveground biomass using multisource remotely sensed data. *Remote Sens.* **2022**, *14*, 1115. [CrossRef]
45. Utari, D.; Kamal, M.; Sidik, F. Above-ground biomass estimation of mangrove forest using WorldView-2 imagery in Perancak Estuary, Bali. *IOP Conf. Ser. Earth Environ. Sci.* **2020**, *500*, 012011. [CrossRef]
46. Zhang, L.; Yin, X.; Wang, Y.; Chen, J. Aboveground biomass mapping in SemiArid forests by integrating airborne LiDAR with Sentinel-1 and Sentinel-2 Time-Series Data. *Remote Sens.* **2024**, *16*, 3241. [CrossRef]
47. Moghimi, A.; Darestani, A.T.; Mostofi, N.; Fathi, M.; Amani, M. Improving forest above-ground biomass estimation using genetic-based feature selection from Sentinel-1 and Sentinel-2 data (case study of the Noor forest area in Iran). *Kuwait J. Sci.* **2024**, *51*, 100159. [CrossRef]
48. Xu, X.; Yang, J.; Qi, S.; Ma, Y.; Liu, W.; Li, L.; Lu, X.; Liu, Y. Estimation of forest aboveground biomass using Sentinel-1/2 synergized with extrapolated parameters from LiDAR data and analysis of its ecological driving factors. *Remote Sens.* **2025**, *17*, 2358. [CrossRef]

Disclaimer/Publisher's Note: The statements, opinions and data contained in all publications are solely those of the individual author(s) and contributor(s) and not of MDPI and/or the editor(s). MDPI and/or the editor(s) disclaim responsibility for any injury to people or property resulting from any ideas, methods, instructions or products referred to in the content.